Model dependence of the γZ dispersion correction to the parity-violating asymmetry in elastic ep scattering

Mikhail Gorchtein,[1,*] C. J. Horowitz,[1] and Michael J. Ramsey-Musolf[2,†]

[1]*Center for Exploration of Energy and Matter, Physics Department, Indiana University, Bloomington, Indiana 47403, USA*

[2]*Department of Physics, University of Wisconsin-Madison, Madison, Wisconsin 53706, USA and Kellogg Radiation Laboratory, California Institute of Technology, Pasadena, California 91125, USA*

(Received 1 March 2011; revised manuscript received 1 June 2011; published 29 July 2011)

We analyze the dispersion correction to elastic parity violating electron-proton scattering due to γZ exchange. In particular, we explore the theoretical uncertainties associated with modeling contributions of hadronic intermediate states. Taking into account constraints from low- and high-energy, parity-conserving electroproduction measurements, choosing different models for contributions from the nonresonant processes, and performing the corresponding flavor rotations to obtain the electroweak amplitude, we arrive at an estimate of the uncertainty in the total contribution to the parity-violating asymmetry. At the kinematics of the Q-Weak experiment, we obtain a correction to the asymmetry equivalent to a shift in the proton weak charge of (0.0054 ± 0.0020). This should be compared to the value of the proton's weak charge of $Q_W^p = 0.0713 \pm 0.0008$ that includes Standard Model contributions at tree level and one-loop radiative corrections. Therefore, we obtain a new Standard Model prediction for the parity-violating asymmetry in the kinematics of the Q-Weak experiment of $(0.0767 \pm 0.0008 \pm 0.0020_{\gamma Z})$. The latter error leads to a relative uncertainty of 2.8% in the determination of the proton's weak charge and is dominated by the uncertainty in the isospin structure of the inclusive cross section. We argue that future parity-violating inelastic ep asymmetry measurements at low to moderate Q^2 and W^2 could be exploited to reduce the uncertainty associated with the dispersion correction. Because the corresponding shift and error bar decrease monotonically with decreasing beam energy, a determination of the proton's weak charge with a lower-energy experiment or measurements of "isotope ratios" in atomic parity violation could provide a useful cross-check on any implications for physics beyond the Standard Model derived from the Q-Weak measurement.

DOI: 10.1103/PhysRevC.84.015502 PACS number(s): 12.15.Lk, 11.55.Fv, 12.40.Vv, 13.85.Dz

I. INTRODUCTION

Precise measurements of low-energy observables can provide powerful probes of physics beyond the Standard Model that complement high-energy collider studies [1,2]. In particular, measurements of parity-violating (PV) observables in atomic physics and electron scattering have provided key tests of the neutral weak current sector of the Standard Model and constrained possible new physics in this sector [2–5]. In this work, we consider PV elastic scattering of longitudinally polarized electrons from hydrogen, which is the subject of the Q-Weak experiment at the Jefferson Lab (JLab) [6]. This experiment draws on a rich history of PV electron scattering (PVES) at various facilities and aims to provide the most precise determination of Q_W^p, the weak charge of the proton, ever made.

In PVES, the weak charge is operationally defined through the forward scattering limit of the PV asymmetry:

$$A^{\rm PV} = \frac{\sigma_+ - \sigma_-}{\sigma_+ + \sigma_-} = \frac{G_F t}{4\sqrt{2}\pi\alpha_{em}} \frac{W^{\rm PV}}{W^{\rm EM}}, \tag{1}$$

where the ratio of response functions is defined below. Here and in the rest of the article, G_F denotes the Fermi constant, as taken from the muon lifetime (often denoted by G_μ). The weak charge–defined as a static property of the proton–is then the leading term the expansion of the ratio $W^{\rm PV}/W^{\rm EM}$ in powers of $t = -q^2$:

$$Q_W^p = \lim_{t\to 0} \frac{W^{\rm PV}}{W^{\rm EM}}\bigg|_{E=0}, \tag{2}$$

where the reason for specifying zero beam energy E becomes apparent below. In the one-boson exchange (OBE) approximation, the weak charge is just given by

$$Q_W^p\big|_{\rm OBE} = -2\,[2C_{1u} + C_{1d}]\,, \tag{3}$$

where the C_{1q} characterize the effective four-fermion PV electron-quark interaction

$$\mathcal{L} = \frac{G_F}{\sqrt{2}}[\bar{e}\gamma^\mu\gamma_5 e(C_{1u}\bar{u}\gamma_\mu u + C_{1d}\bar{d}\gamma_\mu d) + \bar{e}\gamma^\mu e(C_{2u}\bar{u}\gamma_\mu\gamma_5 u + C_{2d}\bar{d}\gamma_\mu\gamma_5 d)]. \tag{4}$$

In the Standard Model, it is possible to make precise predictions for the C_{1q}, including the effects of $\mathcal{O}(\alpha)$ electroweak radiative corrections [5,7,8]. These corrections include the effects of one-loop contributions to the gauge boson and fermion propagators and gauge boson-fermion vertices. Ultraviolet (UV) divergences are removed through renormalization, and in what follows we use the modified minimal subtraction ($\overline{\rm MS}$) scheme for doing so.

Additional, UV-finite corrections arise from the two-boson exchanges ("box graphs"): ZZ, W^+W^-, γZ, and $\gamma\gamma$. Those involving two heavy vector bosons are dominated by loop momenta of order M_Z and are properly included in the

*mgorshte@indiana.edu
†mjrm@physics.wisc.edu

TABLE I. Estimates for the dispersion γZ correction obtained in various works. Originally, Gorchtein and Horowitz in Ref. [11] only quoted the value of the dispersion γZ correction $\approx 6\%$, as calculated relative to $1 - 4\sin^2\theta_W(0) \approx 0.05$. This corresponds to the number given in the table.

Ref. [11]	Ref. [15]	Ref. [17]	This work
$(3 \pm 3) \times 10^{-3}$	$(4.7^{+1.1}_{-0.4}) \times 10^{-3}$	$(5.7 \pm 0.9) \times 10^{-3}$	$(5.4 \pm 2.0) \times 10^{-3}$

radiatively corrected C_{1q} coefficients. On the other hand, the box graph corrections involving one or more photons are sensitive to low-momentum scales where target-dependent hadronic structure effects may be significant. In what follows, we focus on the $Z\gamma$ box correction. For a review of recent work on the $\gamma\gamma$ corrections, see Ref. [9].

Recently, the γZ box graph contribution has been the subject of renewed scrutiny. In Refs. [5,7,10], the short-distance part of this correction was computed, confirming the earlier computation of Ref. [8]. It carries a logarithmic dependence on the hadronic scale, $\Lambda_{\rm had}$, with the latter requiring the presence of a "low-energy constant" $C_{\gamma Z}(\Lambda_{\rm had})$ to yield a result independent of the hadronic matching scale. The authors of Ref. [5,7] assigned a generous error to $C_{\gamma Z}(\Lambda_{\rm had})$ associated with the difficult-to-compute long-distance hadronic effects.

The authors of Ref. [11] subsequently observed that there exists an additional contribution from the γZ box graph that grows with the electron beam energy and that is independent of the hadronic cutoff parameter.[1] Given the energy dependence of this "dispersion correction," it is more appropriate to consider it as a new term in the PV asymmetry than as a contribution to the weak charge that is nominally a static property of the proton. Nevertheless, in the forward limit of Eq. (2), its effect is to shift the apparent value of Q_W^p. Moreover, unlike the short-distance and $C_{\gamma Z}(\Lambda_{\rm had})$ terms that are suppressed by $1 - 4\sin^2\theta_W \approx 0.07$, the energy-dependent correction is not accidentally suppressed. For the energy of the Q-Weak experiment, the authors of Ref. [11] estimated that the correction was several percent, raising the possibility that the estimated theoretical uncertainty in the PV asymmetry could be larger than given in Refs. [5,7].

A follow-up study [15] repeated the computation of Refs. [11,16] using a somewhat different hadronic model framework and drawing upon recent structure function measurements carried out at the JLab. These authors argued that the expressions used in Ref. [11] contained numerical errors but nonetheless obtained a quantitatively similar result for the size of the correction. An estimate of the uncertainty in the correction was also provided, suggesting that the theoretical uncertainty associated with the energy-dependent term is well below the uncertainty quoted in Refs. [5,7]. Recently, another study of this correction was reported in Ref. [17]. The latter work employed yet another parametrization of virtual photoabsorption data from JLab, and a different treatment of the isospin structure and of the uncertainty was applied. The results are consistent with those of Ref. [15] with error bars that are also smaller than those of Refs. [5,7]. We review these works in greater detail below. For the moment, we display in Table I the results of the previously mentioned studies along with the results of this work. While all of the recent results (ours and Refs. [15,17]) are consistent within quoted error bars, we obtain a larger uncertainty by roughly a factor of two. As we discuss below, this larger theory uncertainty results from taking into account hadronic model-dependence in computing the γZ dispersion correction.

Obtaining a robust theoretical prediction for $A^{\rm PV}$ in the Standard Model is essential for the proper interpretation of the asymmetry in terms of possible contributions from physics beyond the Standard Model. In light of the recent history and disagreements in the literature on the question of the γZ box correction, we revisit here the computations of Refs. [11,15–17]. Our goal is threefold. First, we seek to clarify the apparent disagreements about the numerical factors in the analytic expressions for the energy-dependent part of the γZ correction. Second, we attempt to provide an estimate of the theoretical uncertainty associated with hadronic modeling required for its computation. While the study of Ref. [15] included an uncertainty associated with the experimental data used as input for the calculation, no estimate of the theoretical error related to the choice of model framework was given. Finally, we discuss additional experimental input that would be useful to improve the reliability of the calculated correction.

The remainder of our treatment of these points is organized as follows. Section II outlines the elastic electron-nucleon scattering kinematics and observables that are analyzed to one-loop order. In Sec. III, we derive a forward dispersion relation for the dispersion corrections. In Sec. IV, we discuss the input in these sum rules, perform an isospin decomposition of the inclusive electroproduction data, and isospin-rotate these data to obtain the inclusive PV data. We combine different data sets to obtain an estimate of the uncertainty associated with such rotation in the flavor space. Detailed discussion of the isospin rotation of the resonant contributions is reported in the Appendix. In Sec. V, we present our results for the dispersion correction $\Box_{\gamma Z}$ and the respective theory uncertainty at the kinematics of the Q-Weak experiment. Section VI is dedicated to the study of the t dependence of the dispersion correction that is important for translating the value obtained from dispersion relation in the exact forward direction to the experimental kinematics. In Sec. VII, we compare the existing calculations of the energy-dependent dispersion γZ correction to the weak charge of the proton in detail. We close the article with a short summary in Sec. VIII.

II. PVES IN THE FORWARD-SCATTERING REGIME

We consider elastic scattering of massless electrons off a nucleon, $e(k) + N(p) \to e(k') + N(p')$, in the presence

[1] For related work considering the effects of the γZ box graph away from the forward limit—relevant to the strange quark form factor determinations—see Refs. [12–14].

of parity violation (and in absence of CP violation). The scattering amplitude T can be cast in the following form involving six scalar amplitudes $f_i(\nu, t)$, $i = 1, 2, \ldots, 6$,

$$\begin{aligned} T = & \frac{4\pi\alpha_{em}}{-t}\bar{u}(k')\gamma_\mu u(k) \\ & \times \bar{N}(p')\left[f_1\gamma^\mu + f_2 i\sigma^{\mu\alpha}\frac{\Delta_\alpha}{2M} + f_3\frac{P^\mu \not{K}}{M^2}\right]N(p) \\ & - \frac{G_F}{2\sqrt{2}}\bar{u}(k')\gamma_\mu\gamma_5 u(k)\bar{N}(p')\left[f_4\gamma^\mu + f_5 i\sigma^{\mu\alpha}\frac{\Delta_\alpha}{2M}\right]N(p) \\ & - \frac{G_F}{2\sqrt{2}} f_6\,\bar{u}(k')\gamma_\mu u(k)\bar{N}(p')\gamma^\mu\gamma_5 N(p), \end{aligned} \tag{5}$$

where only electromagnetic and weak neutral currents are considered. G_F stands for the Fermi constant, as taken from the muon lifetime, according to the $\overline{\text{MS}}$ scheme. The amplitudes $f_{1,2,3}$ are parity conserving (PC), and $f_{4,5,6}$ are explicitly PV. Above, k (k') stands for the initial (final) electron momenta, and p (p') for the initial (final) nucleon momenta, respectively, and M denotes the mass of the nucleon (we take $M_n \approx M_p \equiv M$). All six amplitudes are functions of energy $\nu = \frac{P\cdot K}{M}$ (with $K = \frac{k+k'}{2}$ and $P = \frac{p+p'}{2}$) and the elastic momentum transfer is $t = \Delta^2 < 0$, with $\Delta = k - k' = p' - p$. At tree level (OBE) and to leading order in G_F and α_{em}, the amplitudes f_i reduce to the electromagnetic and weak form factors of the nucleon (the index N takes values p, n denoting proton and neutron, respectively),

$$\begin{aligned} f_1^{N,\text{OBE}}(\nu, t) &= \mathcal{F}_1^{\gamma N}(t), \\ f_2^{N,\text{OBE}}(\nu, t) &= \mathcal{F}_2^{\gamma N}(t), \\ f_3^{N,\text{OBE}}(\nu, t) &= 0, \\ f_4^{N,\text{OBE}}(\nu, t) &= g_A^e\mathcal{F}_1^{ZN}(t), \\ f_5^{N,\text{OBE}}(\nu, t) &= g_A^e\mathcal{F}_2^{ZN}(t), \\ f_6^{N,\text{OBE}}(\nu, t) &= g_V^e G_{A,N}^e(t)\,. \end{aligned} \tag{6}$$

Above, $g_V^e = -(1 - 4\sin^2\theta_W)$ and $g_A^e = 1$. Radiative corrections induce terms $\delta f_i \sim \alpha_{em}$, leading generically to $f_i = f_i^{\text{OBE}}(t) + \delta f_i(\nu, t)$. We denote the usual Dirac (Pauli) form factors by $\mathcal{F}_{1,2}^{\gamma N}$, respectively, and the nucleon axial form factor at tree level by $G_{A,N}^e$. Similarly, $\mathcal{F}_{1,2}^{ZN}$ stand for the form factors describing the vector coupling of the Z to the nucleon. One introduces the conventional combinations,

$$\begin{aligned} G_M^\gamma &= f_1^N + f_2^N, \\ G_E^\gamma &= f_1^N - \tau f_2^N, \\ G_M^Z &= \frac{1}{g_A^e}\left(f_4^N + f_5^N\right), \\ G_E^Z &= \frac{1}{g_A^e}\left(f_4^N - \tau f_5^N\right), \end{aligned} \tag{7}$$

with $\tau = \frac{-t}{4M^2}$. In absence of radiative corrections, these amplitudes reduce to the electroweak Sachs form factors $G_{E,M}^{\gamma,Z}$. In terms of these generalized form factors, the unpolarized cross section on a nucleon target N can be written as

$$\frac{d\sigma^N}{d\Omega_{\text{Lab}}} = \frac{4\alpha_{em}^2\cos^2\frac{\theta}{2}}{t^2}\frac{E'^3}{E}\frac{\tau\sigma_R^N}{\varepsilon(1+\tau)}, \tag{8}$$

with θ the electron lab scattering angle, E (E') the incoming (outgoing) electron lab energy, and $\varepsilon = [1 + 2(1+\tau)\tan^2\frac{\theta}{2}]^{-1}$ the virtual photon longitudinal polarization parameter. The reduced cross section σ_R^N, up to and including terms of order α_{em}, reads

$$\sigma_R^N = \left|G_M^\gamma\right|^2 + \frac{\varepsilon}{\tau}\left|G_E^\gamma\right|^2 + 2\varepsilon\frac{\nu}{M}\left(G_M^\gamma + \frac{1}{\tau}G_E^\gamma\right)\text{Re}\,f_3^N. \tag{9}$$

In what follows, we concentrate on the case of electron-proton scattering. Therefore, we understand $N = p$ everywhere and suppress the index N in all expressions, unless explicitly stated otherwise.

The PV asymmetry is defined in Eq. (1) with the ratio of the response functions given by

$$\frac{W^{\text{PV}}}{W^{\text{EM}}} = \text{Re}\frac{G_M^\gamma G_M^{Z*} + \frac{\varepsilon}{\tau}G_E^\gamma G_E^{Z*} + \varepsilon\frac{\nu}{M}f_3\left(G_M^{Z*} + \frac{1}{\tau}G_E^{Z*}\right) + \frac{\varepsilon'}{\tau}G_M^\gamma f_6^*}{\sigma_R}\,. \tag{10}$$

Here $\sigma_\pm$ are the cross sections for positive and negative helicity electrons, and $\varepsilon' = \sqrt{\tau(1+\tau)(1-\varepsilon^2)}$.

Because we are interested in very forward scattering angles $\theta \approx 8^\circ$ corresponding to the Q-Weak kinematics [6], thus $\tau < 10^{-3}$, the expressions for the cross section and PV asymmetry can be further simplified.

For the reduced cross section the leading contribution in Eq. (9) comes from the G_E^2 term, and we obtain

$$\sigma_R = \frac{1}{\tau}\left(\mathcal{F}_1^\gamma\right)^2\left(1 + \tau\delta_{\text{kin}}^\sigma + 2\text{Re}\bar{\delta}_{RC}^\sigma\right) + 2\text{Re}\Box_{\gamma\gamma}. \tag{11}$$

The three distinct corrections quoted above are defined as follows: $\delta_{\text{kin}}^\sigma$ is a kinematic correction that arises at tree level due to the magnetic part and other subleading kinematic effects of order $\tau, (1-\epsilon)$, which do not contain $\mathcal{O}(\alpha_{em})$ effects; $\bar{\delta}_{RC}^\sigma$ stands for order $\mathcal{O}(\alpha_{em})$ corrections that are energy-independent (such as vacuum polarization, self-energy, and vertex corrections); finally, $\Box_{\gamma\gamma}$ denotes the two-photon exchange correction that is an energy-dependent $\mathcal{O}(\alpha_{em})$ correction.

Similarly, for the PV asymmetry the leading order contribution in Eq. (10) originates from the $G_E^{Z*}G_E^\gamma$ term.

As discussed in Ref. [5], the Standard Model prediction for the PV asymmetry in the forward regime can be expressed as

$$A^{\rm PV} = \frac{G_F t}{4\sqrt{2}\pi\alpha_{\rm em}}\left[(1+\Delta\rho+\Delta_e)(1-4\sin^2\hat{\theta}_W(0)+\Delta_e') + \Box_{WW}+\Box_{ZZ}+\Box_{\gamma Z}\right]+\ldots, \quad (12)$$

where $\hat{\theta}_W(0)$ is the running weak mixing angle in the $\overline{\rm MS}$ scheme at zero momentum transfer [7]. The correction $\Delta\rho$ is a universal radiative correction to the relative normalization of the neutral and charged current amplitudes; the Δ_e and Δ_e' give, respectively, nonuniversal corrections to the axial vector Zee and γee couplings; the $\Box_{VV}$ for $V = W, Z, \gamma$ give the nonuniversal box graph corrections; and the "$+\cdots$" indicate terms that vanish with higher powers of t in the forward limit, such as those arising from the magnetic and strange quark form factors and the two-photon dispersion correction, $\Box_{\gamma\gamma}$. The weak charge of the proton, considered as a static property, is given by the quantity in the squark brackets in the zero-energy limit.

Within the radiative corrections, the TBE effects are separated explicitly. This is done because the TBE corrections, unlike other corrections in the above equation, are in general ν and t dependent. In particular, the ν (or ε) dependence of the $\gamma\gamma$-box is believed to be responsible for the discrepancy between the Rosenbluth and polarization transfer data for G_E^γ/G_M^γ [18]. It should be noted that in the exact forward direction $\Box_{\gamma\gamma}$ vanishes as a consequence of electromagnetic gauge invariance.

The WW and ZZ-box diagrams were first considered in [8] and subsequently investigated in Refs. [5,19]. The contribution from $\Box_{WW}$ in particular is relatively large. Both corrections are ν independent at any hadronic energy scale because they are dominated by exchange of hard momenta in the loop $\sim M_W, M_Z$. Higher-order perturbative QCD corrections to $\Box_{WW}$ and $\Box_{ZZ}$ were computed in Ref. [5], and the overall theoretical uncertainty associated with these contributions is well below the expected uncertainty of the Q-Weak experiment.

In contrast to $\Box_{WW}$ and $\Box_{ZZ}$, $\Box_{\gamma Z}$ receives substantial contributions from loop momenta at all scales. For the electron energy-independent contribution, this situation leads to the presence of a large logarithm $\ln M_Z/\Lambda_{\rm had}$, where $\Lambda_{\rm had}$ is a typical hadronic scale [5,8,19]. Because the asymmetry must be independent of the latter, $\Box_{\gamma Z}$ includes also a "low-energy constant" $C_{\gamma Z}(\Lambda_{\rm had})$ whose hadronic scale dependence compensates for that appearing in the logarithm. An analogous $W\gamma$ box correction enters the vector current contribution to neutron and nuclear β decay. Importantly for the PV asymmetry, these energy-independent γZ box contributions are suppressed by $1-4\sin^2\theta_W$, thereby suppressing the associated theoretical uncertainty.

In Ref. [11], the γZ-box contribution was reexamined in the framework of dispersion relations and it was found that it possesses a considerable energy dependence, so that at energies in the GeV range its value can differ significantly from that found at zero energy. Moreover, the energy-dependent correction contains a term that is not $1-4\sin^2\theta_W$ suppressed, so the theoretical uncertainty associated with hadronic-scale contributions is potentially more significant. This energy dependence comes through contributions from hadronic energy range inside the loop that cannot be calculated reliably using perturbative techniques.

At present, a complete first-principles computation is not feasible, forcing one to rely on hadronic modeling. For a proper interpretation of the PV asymmetry, it is thus important to investigate the theoretical hadronic model uncertainty. The remainder of the paper is devoted to this task. In so doing, we attempt to reduce this model uncertainty by relating–wherever possible–contributions from hadronic intermediate states to experimental PC electroproduction data through the use of a dispersion relation and isospin rotation. As a corollary, we also identify future experimental measurements, such as those of the PV inelastic asymmetry in the regime of moderate Q^2 and W, that could be helpful in reducing the theoretical uncertainty.

III. DISPERSION CORRECTIONS

To calculate the real part of the γZ direct and crossed box diagrams shown in Fig. 1, we follow [11] and adopt a dispersion relation formalism. We start with the calculation of the imaginary part of the direct box (the crossed box contribution to the real part will be calculated using crossing),

$$\mathrm{Im}T_{\gamma Z} = -\frac{G_F}{\sqrt{2}}\frac{e^2}{(2\pi)^3}\int\frac{d^3\vec{k}_1}{2E_1}\frac{l_{\mu\nu}\cdot W_{\gamma Z}^{\mu\nu}}{Q^2\left(1+Q^2/M_Z^2\right)}, \quad (13)$$

where $Q^2 = -(k-k_1)^2$ denotes the virtuality of the exchanged photon and Z (in the forward direction they carry exactly the same Q^2), and we explicitly set the intermediate electron on shell. In the center of mass of the (initial) electron and proton, one has $E_1 = \frac{s-W^2}{2\sqrt{s}}$, with s the full c.m. energy squared and W the invariant mass of the intermediate hadronic state. Note that for on-shell intermediate states, the exchanged bosons are always spacelike.

The leptonic tensor is given by

$$l_{\mu\nu} = \bar{u}(k')\gamma_\nu \not{k}_1 \gamma_\mu\left(g_V^e + g_A^e\gamma_5\right)u(k). \quad (14)$$

We next turn to the lower part of the diagrams in Fig. 1. The blobs stand for an inclusive sum over all possible hadronic intermediate states, starting from the ground state (i.e., the nucleon itself) and on to a sum over the whole nucleon photoabsorption spectrum. The case of the elastic hadronic intermediate state was considered in Ref. [20]. Here we concentrate on the inelastic contribution. Such contributions arise from the absorption of a photon (weak boson). In electrodynamics, for a given material, the relation between

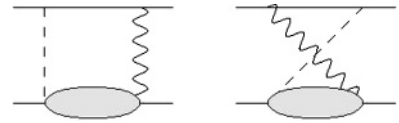

FIG. 1. Direct and crossed diagrams for γZ exchange. Dashed lines correspond to an exchange of a Z boson, and wavy lines to an exchange of a photon. The blob stands for an inclusive sum over intermediate hadronic states.

its refraction coefficient and the dependence of the latter on the photon frequency (i.e., dispersion) on one hand and the photoabsorption spectrum of that material on the other hand is historically called a dispersion relation. It is exactly this dependence of the forward-scattering amplitude $f_4(\nu, 0)$ [see Eq. (5)] on the energy that arises from its relation to the electroweak $\gamma(Z)$-absorption spectrum that is the scope of an investigation in this work. This explains the origin of the term "dispersion correction" used for the inelastic contributions to the γZ-box correction.

In the forward direction, the imaginary part of the doubly virtual "Compton scattering" ($\gamma^* p \to Z^* p$) amplitude is given in terms of the interference structure functions $F_{1,2,3}^{\gamma Z}(x, Q^2)$, with $x = \frac{Q^2}{2Pq}$ the Bjorken variable. Making use of gauge invariance of the leptonic tensor, we have

$$\frac{1}{2\pi} W_{\gamma Z}^{\mu\nu} = -g^{\mu\nu} F_1^{\gamma Z} + \frac{P^\mu P^\nu}{Pq} F_2^{\gamma Z} + i\epsilon^{\mu\nu\alpha\beta} \frac{P_\alpha q_\beta}{Pq} F_3^{\gamma Z}. \tag{15}$$

Contracting the two tensors, one obtains after a little algebra two contributions that correspond, respectively, to the axial and vector couplings of the Z to the electron,

$$\begin{aligned} \mathrm{Im}\Box_{\gamma Z_A}(\nu) &= \alpha_{em} g_A^e \int_{W_\pi^2}^{s} \frac{dW^2}{(s-M^2)^2} \int_0^{Q^2_{\max}} \frac{dQ^2}{1+\frac{Q^2}{M_Z^2}} \\ &\quad \times \left[F_1^{\gamma Z} + \frac{s(Q^2_{\max} - Q^2)}{Q^2(W^2 - M^2 + Q^2)} F_2^{\gamma Z} \right], \\ \mathrm{Im}\Box_{\gamma Z_V}(\nu) &= -\alpha_{em} g_V^e \int_{W_\pi^2}^{s} \frac{dW^2}{(s-M^2)^2} \int_0^{Q^2_{\max}} \frac{dQ^2}{1+\frac{Q^2}{M_Z^2}} \\ &\quad \times \left(\frac{2(s-M^2)}{W^2 - M^2 + Q^2} - 1 \right) F_3^{\gamma Z}, \end{aligned} \tag{16}$$

where the imaginary parts Im$\Box$ will appear in a dispersion relation for the real parts in Eq. (20) below. The full correction is the sum of the two,

$$\mathrm{Im}\Box_{\gamma Z}(\nu) = \mathrm{Im}\Box_{\gamma Z_A}(\nu) + \mathrm{Im}\Box_{\gamma Z_V}(\nu). \tag{17}$$

In Eqs. (16), $W_\pi^2 = (M + m_\pi)^2$ stands for the pion production threshold, and the Q^2-integration is constrained below a maximum value,

$$Q^2_{\max} = \frac{(s-M^2)(s-W^2)}{s}, \tag{18}$$

as a condition of on-shell intermediate states for an imaginary part calculation. Equation (16) is in agreement with Refs. [15,17]. In particular, we confirm the correctness of the claim made in Ref. [15] that in Ref. [11] a factor of 2 was missing.

To write the dispersion relation for the function $\Box_{\gamma Z}(\nu)$, one should consider its behavior under crossing. We distinguish two contributions, $\Box_{\gamma Z_V}$ and $\Box_{\gamma Z_A}$ that have different crossing behavior [11]:

$$\begin{aligned} \Box_{\gamma Z_A}(-\nu) &= -\Box_{\gamma Z_A}(\nu), \\ \Box_{\gamma Z_V}(-\nu) &= +\Box_{\gamma Z_V}(\nu). \end{aligned} \tag{19}$$

Correspondingly, the two contributions obey dispersion relations of two different forms,

$$\begin{aligned} \mathrm{Re}\Box_{\gamma Z_A}(\nu) &= \frac{2\nu}{\pi} \int_{\nu_\pi}^{\infty} \frac{d\nu'}{\nu'^2 - \nu^2} \mathrm{Im}\Box_{\gamma Z_A}(\nu'), \\ \mathrm{Re}\Box_{\gamma Z_V}(\nu) &= \frac{2}{\pi} \int_{\nu_\pi}^{\infty} \frac{\nu' d\nu'}{\nu'^2 - \nu^2} \mathrm{Im}\Box_{\gamma Z_V}(\nu'), \end{aligned} \tag{20}$$

where the presence or absence of the factor of ν' in the integrands follows from the behavior of the Im$\Box$ under crossing symmetry.

The result in Eq. (20) gives a model-independent relation between the dispersion correction to the weak charge of the proton and the PV structure functions appearing in Eq. (16). This relation does not rely on any assumption, other than the neglect of higher-order radiative corrections and the number of subtractions needed for convergence of the dispersion relation. The advantage for this formulation is that the $F_k^{\gamma Z}$ are, in principle, measurable. However, in absence of any detailed PV inclusive electron-scattering data, the input in the dispersion integral will depend on a model. In the following, we investigate the extent to which this model dependence can be constrained by existing or future experimental data.

IV. INPUT TO THE DISPERSION INTEGRAL

In the previous section, the contribution of the forward hadronic tensor to the box diagram was considered. In this section, we address the possibility of relating the interference hadronic tensor of Eq. (15),

$$W_{\gamma Z}^{\mu\nu} = \frac{1}{2} \int d^4z e^{iqz} \langle N | T \left[J_{em}^\nu(z) J_{NC_V}^\mu(0) \right] | N \rangle, \tag{21}$$

to the pure electromagnetic one,

$$W_{\gamma\gamma}^{\mu\nu} = \frac{1}{2} \int d^4z e^{iqz} \langle N | T \left[J_{em}^\nu(z) J_{em}^\mu(0) \right] | N \rangle. \tag{22}$$

Using unitarity, we rewrite these matrix elements as an inclusive sum over intermediate hadronic states,

$$\begin{aligned} \mathrm{Im} W_{\gamma Z}^{\mu\nu} = \frac{1}{2} \int d^4z e^{iqz} \Bigg[&\sum_X \langle N | J_{em}^\nu(z) | X \rangle \langle X | J_{NC_V}^\mu(0) | N \rangle \\ &+ \sum_X \langle N | J_{NC_V}^\nu(z) | X \rangle \langle X | J_{em}^\mu(0) | N \rangle \Bigg] \end{aligned} \tag{23}$$

and

$$\mathrm{Im} W_{\gamma\gamma}^{\mu\nu} = \frac{1}{2} \int d^4z e^{iqz} \sum_X \langle N | J_{em}^\nu(z) | X \rangle \langle X | J_{em}^\mu(0) | N \rangle, \tag{24}$$

respectively. We now proceed to investigate the possible relationships between the products of transition matrix elements appearing in each inclusive sum (23) and (24).

Theoretically, calculating the full set of contributions to the inclusive sum represents a fundamental difficulty because in QCD, the basis for intermediate states X is infinite, and the matrix elements are nonperturbative. Under certain kinematic conditions, one can organize this basis into leading

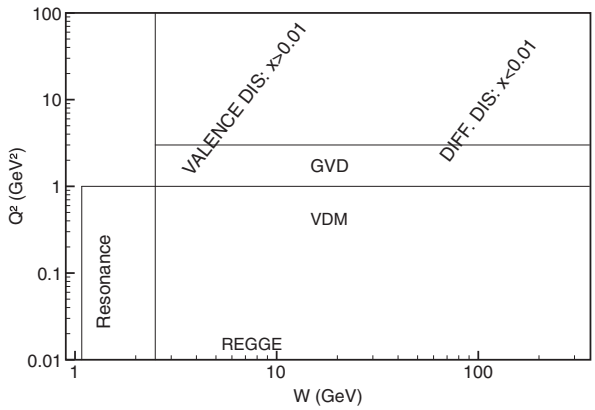

FIG. 2. The plane Q^2 vs W and kinematic regions corresponding roughly to various physical contributions.

and subleading (kinematically suppressed) subsets. We depict this situation schematically in Fig. 2, where we show in the Q^2-W^2 plane the approximate kinematic areas where various mechanisms dominate. At high energy and Q^2, and finite Bjorken x, the leading set of states is $X = q + X'$ (q denotes a quark), where to leading order in $1/Q$, X' is a spectator. Thus, in this regime the electromagnetic (weak) current directly probes a single quark within the nucleon and gives access to the parton distribution functions (deep inelastic scattering, DIS in Fig. 2). At high energy and Q^2, and small x, however, the picture changes, as the leading set is $X = \bar{q}q + N$. In this regime, the photon polarizes the QCD vacuum at the periphery of the hadron, and the resulting $\bar{q}q$ pair forms a color dipole that interacts with the nucleon (diffractive DIS in Fig. 2). This picture was first realized in the vector meson dominance (VDM) model that capitalized on the fact that because vector mesons and the photon have the same quantum numbers, the latter can fluctuate into the former [21,22]. This simple model works quite well at low Q^2 (VDM area in Fig. 2). Such "hadronlike" behavior of a photon in scattering processes also results in the electromagnetic (e.m.) data following the Regge behavior, as a function of W (respective Regge area in Fig. 2). At higher values of Q^2, rescattering effects in vector meson-nucleon scattering become increasingly important but can still be accounted for in what is called the "generalized VDM" (GVDM region in Fig. 2). At low energies, the relevant degrees of freedom are hadronic (that is, highly nonperturbative), $X = N, \pi N, \pi\pi N, N^*, \Delta$, etc. In this regime, the inelastic cross section is typically dominated by resonances on top of a nonresonant background (Resonance area in Fig. 2). The boundaries of each kinematic region are, of course, approximate. Their meaning is that the farther one departs from a kinematical region, the lesser extent to which the respective mechanism works. Consequently, a large area on the W^2-Q^2 plane, which overlaps with all the depicted regions but not covering them completely is the so-called shadow region where none of the mechanisms can be considered as fully dominant.

If data for the γZ interference cross section existed throughout all these distinct regimes, we would not need to know details of any of the aforementioned models. In principle, such data could be obtained with measurements of the PV inelastic asymmetries in the various kinematic regimes shown in Fig. 2. At present, however, either no or very poor data on PV inelastic scattering exist. Consequently, we instead pursue an alternate strategy, endeavoring to make use of extensive data sets for real and virtual photoabsorption that exist through vast kinematic region in energy and Q^2. To that end, we rely on models that adequately describe the photoabsorption cross section in different regimes and for each attempt to establish relationships between the matrix elements $\langle X|J^\mu_{em}|N\rangle$ and $\langle X|J^\mu_{NC}|N\rangle$ for each intermediate hadronic state $|X\rangle$ of definite isospin. We approach this problem by extracting the electromagnetic matrix elements from inclusive e.m. data and then isospin-rotate every such matrix element. We begin with a brief review of the experimental situation and discuss various model descriptions.

A. Real and virtual photoabsorption data

We find that the dispersion integral for $\mathrm{Re}\Box_{\gamma Z}$ is dominated by moderate values of $W \lesssim 5$ GeV and $Q^2 \lesssim 3$ GeV^2 (see Fig. 15 in Sec. V). Consequently, we need to analyze in detail contributions from the resonance regime and portions of what we have called the VDM, GVDM, and Regge regimes. Our goal will be to draw upon existing experimental data for inclusive and semi-inclusive electromagnetic data to infer the γZ interference structure functions that appear in the dispersion integrals. To that end, we first summarize the experimental situation.

(i) Real photoabsorption cross sections have been measured from the pion threshold to very high energies [23–28].

(ii) Virtual photoabsorption data: high-precision data from the JLab E94-110 [29] and the preliminary data from the E00-002 [30] experiments are available in the resonance region; in the DIS region, we quote the data for the DIS structure function F_2 from SLAC NMC Collaboration [31], FNAL E665 Collaborations [32], and DESY H1 Collaboration [33].

While it is equally possible to use structure functions to describe resonance data, in the following we opt to use total photoabsorption cross sections with transverse or longitudinal (for virtual photons only) photon polarization. These cross sections are unambiguously related to the electromagnetic structure functions,

$$\sigma_T^{\gamma p}(W^2, Q^2) = \frac{8\pi^2\alpha}{W^2 - M^2} F_1^{\gamma\gamma}(x, Q^2)$$
$$\sigma_L^{\gamma p}(W^2, Q^2) = \frac{8\pi^2\alpha}{W^2 - M^2}\left[- F_1^{\gamma\gamma}(x, Q^2) + \left(\frac{1}{2x} + \frac{2M^2}{W^2 - M^2 + Q^2}\right) F_2^{\gamma\gamma}(x, Q^2)\right], \quad (25)$$

with the usual Bjorken scaling variable $x = \frac{Q^2}{W^2 - M^2 + Q^2}$. This choice is convenient because in what follows we address transitions between helicity states of the nucleon and resonances, and it is preferable to work with matrix elements of the electromagnetic current with definite helicities. As

is evident from Eq. (25), the two helicity states are mixed in F_2. Similar relations hold between the interference cross sections $\sigma_{T,L}^{\gamma Z,p}(W^2, Q^2)$ and interference structure functions $F_{1,2}^{\gamma Z}(x, Q^2)$. Note that the definition of the transverse and longitudinal polarizations of the photon and the Z-boson are identical because in both cases they are fixed by the lepton kinematics of the reaction $e + p \to e' + X$.

Real photoabsorption data exhibit the following general features: (i) a resonance structure on top of (ii) a smooth nonresonant background between the threshold of pion production and $W \sim 2$–2.5 GeV, and (iii) Regge behavior at high values of W with the cross section that grows slowly with energy, $\sigma_{\rm tot}^{\gamma p} \sim (W^2)^{\alpha_P - 1}$, with $\alpha_P \sim 1.095$ the parameter of the Pomeron:

$$\begin{aligned} \sigma_{\rm tot}^{\gamma p}(W^2) &= \sigma_{\rm res}^{\gamma p}(W^2) + \sigma_{\rm bkgd}^{\gamma p}(W^2), \\ \sigma_{\rm tot}^{\gamma p}(W^2 \to \infty) &\to \sigma_{\rm Regge}^{\gamma p}(W^2) \sim (W^2)^{\alpha - 1}, \end{aligned} \tag{26}$$

where $\alpha = \alpha_P, \alpha_{f_2}$, etc., stand for Pomeron and Regge trajectories. In this work, the most recent fit in terms of two trajectories (Pomeron plus f_2) is used [34]

$$\sigma_{\rm bkgd}^{\gamma p} = f_{\rm thr}\left[(145.0 \pm 2.0)\,\mu b \left(\frac{W^2}{W_0^2}\right)^{-0.5} + (63.5 \pm 0.9)\,\mu b \left(\frac{W^2}{W_0^2}\right)^{\epsilon}\right], \tag{27}$$

with parameter of the Pomeron $\epsilon = 0.097 \pm 0.002$. The threshold factor $f_{\rm thr}$ is necessary to make the continuation of the Regge fit into the resonance region meaningful. In this work, we take it in the same form as in [35]:

$$f_{\rm thr} = 1 - \exp\left[-\frac{W^2 - (M + m_\pi)^2}{M^2}\right]. \tag{28}$$

For virtual photons in the range of W^2, Q^2 of interest here, the picture remains the same, with the Q^2 dependence of the resonance contributions described by the form factors measured for a number of resonances, at least in certain channels.

We next specify two models that provide a smooth extrapolation between the real photoabsorption data and the virtual photoabsorption data and that can to a certain extent be used to describe data all the way up into the diffractive DIS region. The two models differ in the form of the Q^2 dependence of the background contribution:

(i) *Model I*. The model used in Ref. [11] utilized the resonance parameters obtained in Ref. [35] and the nonresonant Regge contribution from Ref. [34] that was fitted to the real photoabsorption data at high energies. The Q^2 dependence of the high-energy part was taken from the hybrid GVD/color dipole (CDP) approach of Ref. [37]. For the estimates of Ref. [11], a simple dipole model with the dipole mass $\Lambda \approx 1$ GeV for all the transition resonance form factors was employed. Because it was found that this simple dipole form fails dramatically throughout the resonance region, we adopt the resonance part from Ref. [38] with a few parameters minimally adjusted to fit the data with the background of a different form, rather the one used in Ref. [38] originally. We list those parameters and the respective changes in Table II.

(ii) *Model II*. To test the sensitivity of our calculations to the specific model, we use another form of the background from the "naive" GVD model of Ref. [39] [cf. Eqs. (3) and (4) of that reference], and we add the resonance contributions from Ref. [38] on top of that. Again, some resonance parameters are slightly adjusted to the background, and all changes are quoted in Table II.

TABLE II. The list of the resonance parameters and their values for Model I and Model II, as compared to the original fit of Ref. [38] (see Table III of that reference). The notation of Ref. [38] was kept.

Parameter	Ref. [38]	Model I	Model II
c_1	2.124	2.24	2.2
c_2	2.569	2.73	2.73
c_4	0.064	0.155	0.155
c_5	0.549	0.549	0.7
c_6	1.914	1.914	2.5
c_7	1.0	1.0	1.5
$A_T^7(0)$	3.419	5	5
$A_L^7(0)$	11	15	15

In Fig. 3 we confront the two models with the total photoabsorption cross section. Model I is shown by solid red lines, Model II by the dashed blue line.

Figures 4–6 display the comparison of the two models with the data for the differential cross section for inclusive electroproduction in the resonance region. Both models in general provide a good description of the data in the resonance region. The areas between the lower and upper thin curves in each plot correspond to the range of values of the helicity amplitudes for the photoexcitation of each resonance included in Models I and II, as given by the PDG [40]. It can be seen that the experimental data are always contained within these areas for $W^2 \leqslant 4$ GeV^2, even without

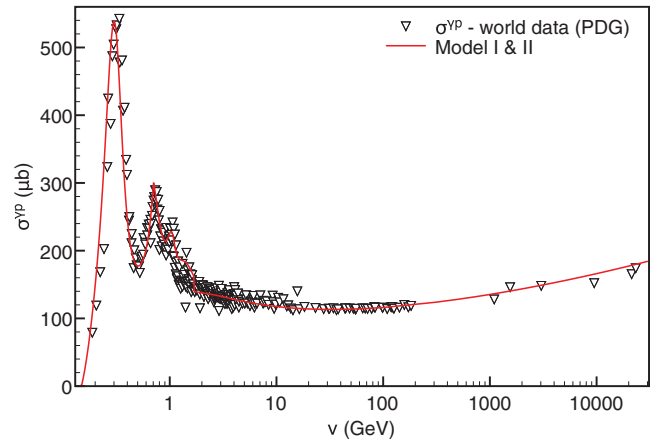

FIG. 3. (Color online) World data on total photoabsorption [23–28] (see Ref. [36] for the complete list) compared to the two models described in the text. The experimental errors are not shown.

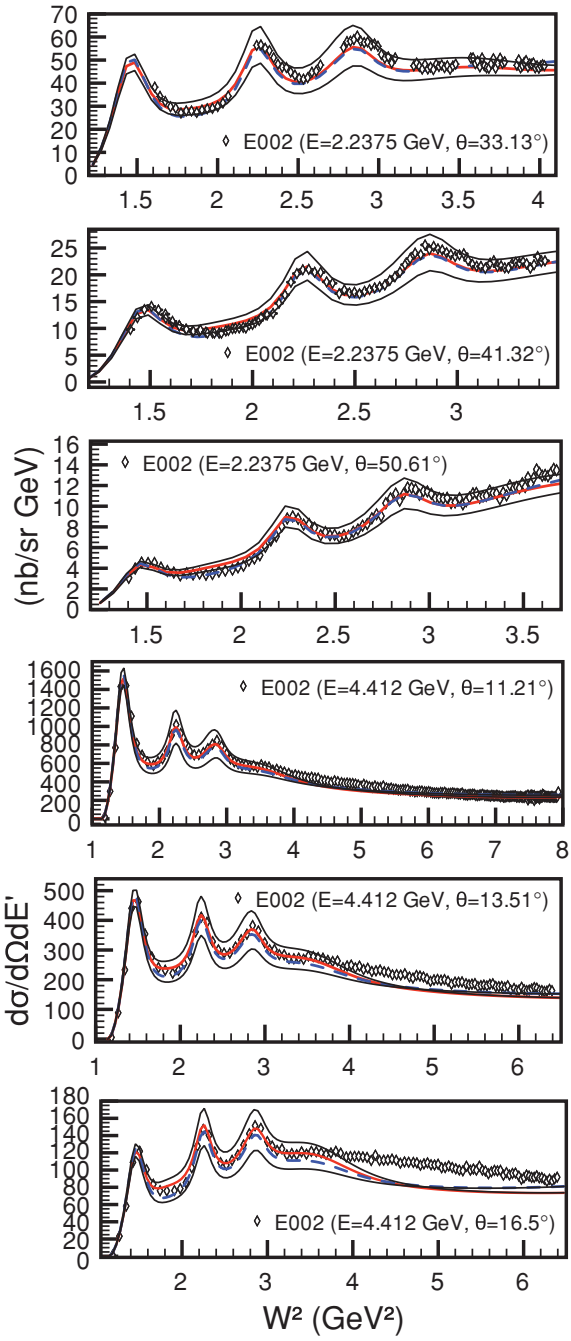

FIG. 4. (Color online) Differential cross-section data in the resonance region from Ref. [30] are shown in comparison with the two models. The experimental errors are not shown. The thick solid line is the result of Model I, and the thick dashed line is the result of Model II. Thin solid lines show the error bar owing to the uncertainties in helicity amplitudes for the photoexcitation of the resonances on the proton, according to Ref. [40].

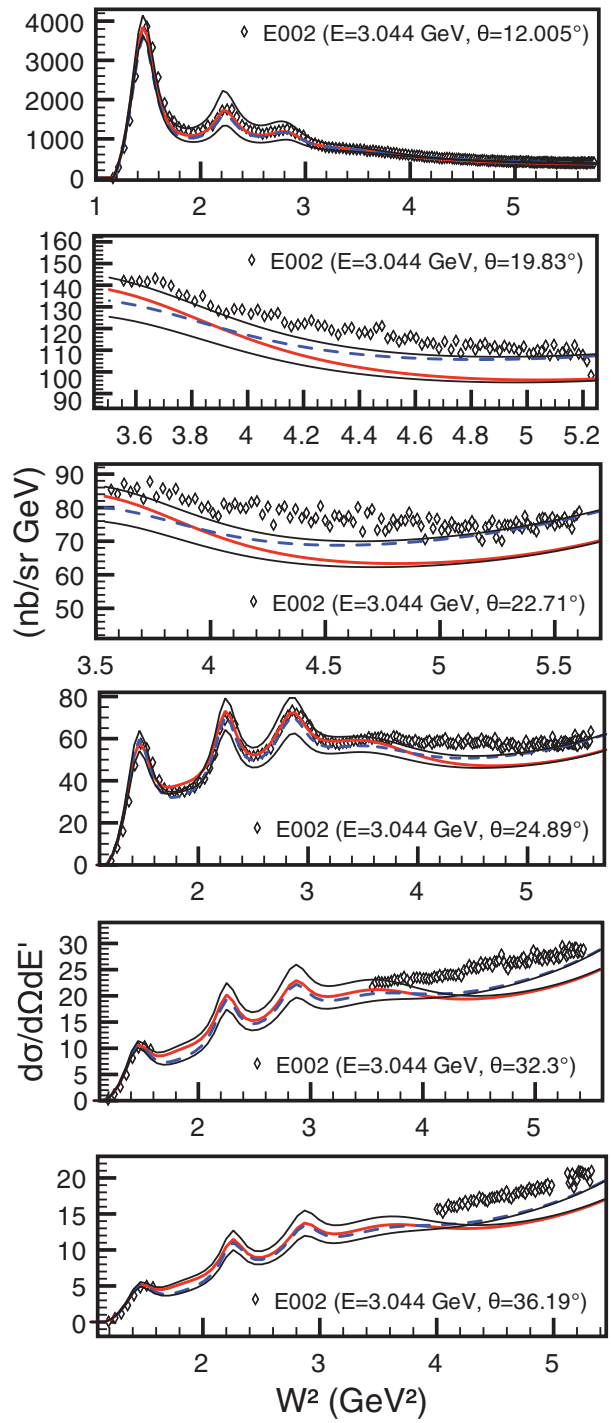

FIG. 5. (Color online) Differential cross-section data in the resonance region from Ref. [30] are shown in comparison with Models I and II. Notation as in Fig. 4.

including the experimental errors. At the same time, we note that just above the resonance region, in the limited range $4\ \text{GeV}^2 \leqslant W^2 \leqslant 6\ \text{GeV}^2$, and at moderate values of Q^2, the background systematically lacks strength. However, we stress that this lack of strength is observed only in very limited range of energies, and the deficit is less than 20%, which makes the impact of this effect on the dispersion correction small.

We next turn to the deep inelastic (DIS) data. For DIS, a natural choice would be to use the PDF parametrizations from MRST or CTEQ, DGLAP-evolved to the necessary value of

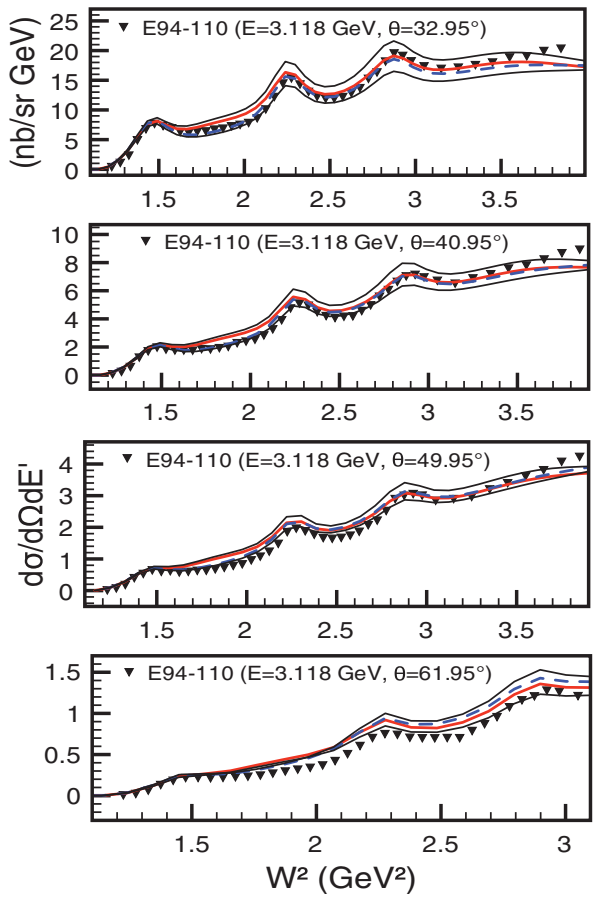

FIG. 6. (Color online) Differential cross-section data in the resonance region from Ref. [29] are shown in comparison with Models I and II. Notation as in Fig. 4.

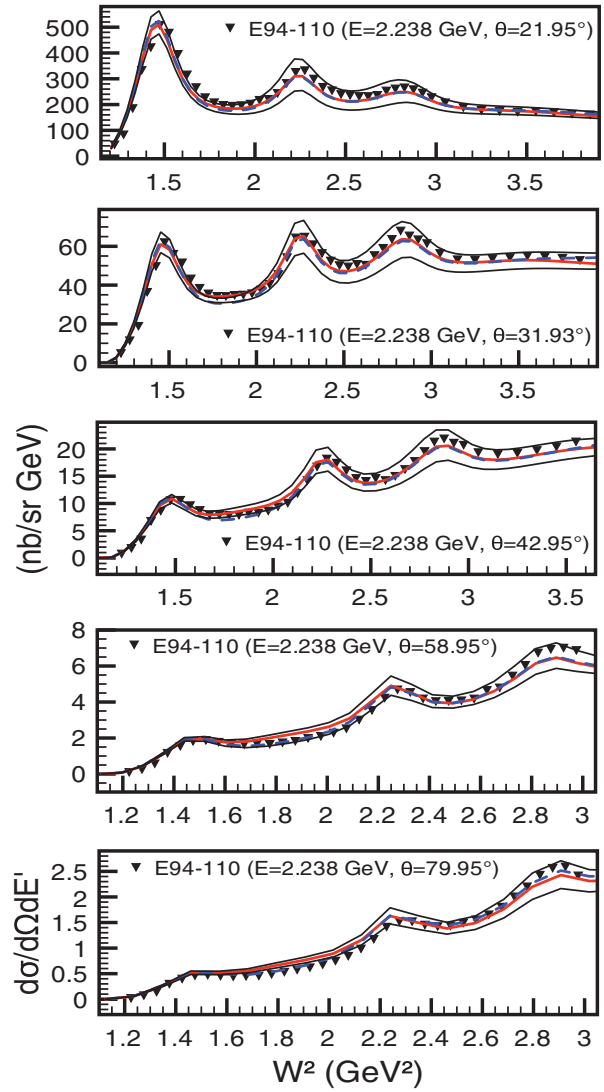

FIG. 7. (Color online) Differential cross-section data in the resonance region from Ref. [29] are shown in comparison with Models I and II. Notation as in Fig. 4.

Q^2. However, this is only applicable at large-enough Q^2, and extrapolating them below $Q^2 = 1$ GeV^2 introduces additional systematic error. In Figs. 10 and 11, the naive GVD model of Ref. [39] (Model II) is shown along with the GVD/CDP model of [37] (Model I). One can see that while the GVD/CDP model reproduces the data in a wide range of x, Q^2, the naive GVD model overshoots the data at large x starting at moderate Q^2, and underestimates the low-x behavior for all Q^2. One needs to keep in mind, however, that both models work reasonably well at moderate Q^2 and large x which give the main contributions to the dispersion correction.

The following comment is in order here. The authors of Ref. [15] argued that our description of the data is unsatisfactory not only in the resonance region but also beyond (cf. Fig. 1 of [15]). While the model of the resonance form factors of Ref. [11] was definitely not accurate (one of the instances on which we improve that calculation in the present work), the model for the background in [11] is exactly the same as that of Model I here. We believe that Figs. 4–11 presented in this section provide abundant evidence of a satisfactory description of the experimental data by our phenomenological model. In view of this, we find it puzzling that Ref. [15] quotes a discrepancy of 40%–50% at Q^2 as low as 0.6 GeV^2 just above the resonance region (cf. the top left panel of Fig. 1 of that reference).

B. Isospin rotation of the resonance contributions

In the Standard Model, the Z and γ hadronic currents are related by means of a simple isospin rotation,

$$\begin{aligned} J^\mu_{em} &= q^{I=0} J^\mu_{I=0} + q^{I=1} J^\mu_{I=1} + q^s J^\mu_s, \\ J^\mu_{NC_V} &= g_V^{I=0} J^\mu_{I=0} + g_V^{I=1} J^\mu_{I=1} + g_V^s J^\mu_s, \end{aligned} \tag{29}$$

with

$$\begin{aligned} J^\mu_{I=0} &= \frac{1}{\sqrt{2}}(\bar{u}\gamma^\mu u + \bar{d}\gamma^\mu d), \\ J^\mu_{I=1} &= \frac{1}{\sqrt{2}}(\bar{u}\gamma^\mu u - \bar{d}\gamma^\mu d), \\ J^\mu_s &= \bar{s}\gamma^\mu s. \end{aligned} \tag{30}$$

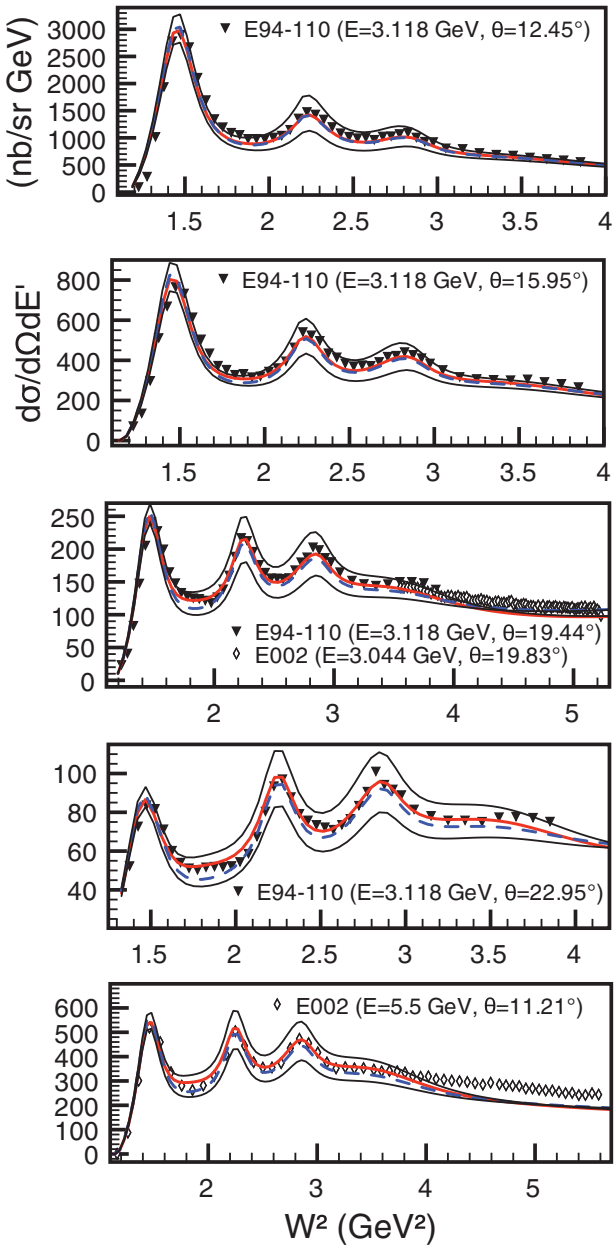

FIG. 8. (Color online) Differential cross-section data in the resonance region from Ref. [29] are shown in comparison with Models I and II. Notation as in Fig. 4.

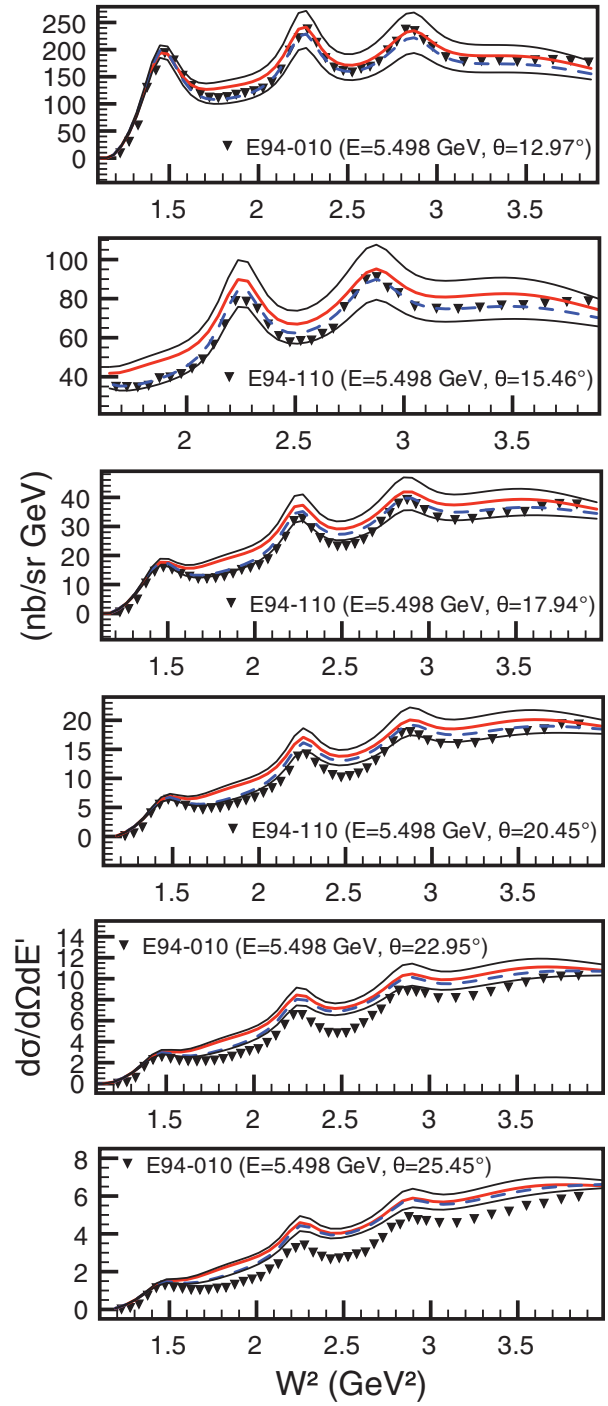

FIG. 9. (Color online) Differential cross-section data in the resonance region from Ref. [29] are shown in comparison with Models I and II. Notation as in Fig. 4.

The e.m. charges given by

$$q^{I=0} = \frac{1}{3\sqrt{2}}, \quad q^{I=1} = \frac{1}{\sqrt{2}}, \quad q^{s} = -\frac{1}{3}, \tag{31}$$

whereas the weak charges are

$$g_V^{I=0} = -\frac{1}{\sqrt{2}}\frac{4}{3}s^2\theta_W,$$
$$g_V^{I=1} = \frac{1}{\sqrt{2}}(2 - 4s^2\theta_W),$$
$$g_V^{s} = -1 + \frac{4}{3}s^2\theta_W,$$

with $s^2\theta_W$ being a shorthand for $\sin^2\theta_W$ (for purposes of this argument). This isospin decomposition is used to relate weak proton form factors to the proton and neutron electromagnetic form factors,

$$\langle p|J^{\mu}_{NC,V}|p\rangle = (1 - 4s^2\theta_W)\langle p|J^{\mu}_{em}|p\rangle - \langle n|J^{\mu}_{em}|n\rangle, \tag{32}$$

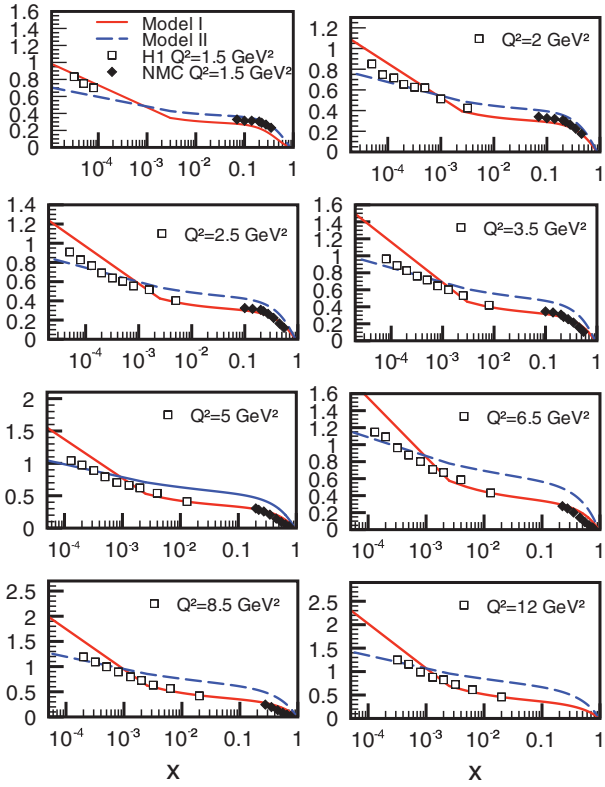

FIG. 10. (Color online) Comparison of the x dependence of the DIS structure function $F_2(x, Q^2)$ at fixed Q^2 and as a function of x, in GVD/CDP model of Ref. [37] (solid lines) and the naive GVD model of [39] (dashed lines) to the low-x DIS data of the H1 Collaboration [33]. The experimental errors are not shown.

where we neglected strangeness contributions that are generally small [41].

The above relation is valid for transitions to $I = \frac{1}{2}$ resonances as well:

$$\langle X|J^{\mu}_{NC,V}|p\rangle = (1 - 4s^2\theta_W)\langle X|J^{\mu}_{em}|p\rangle - \langle X|J^{\mu}_{em}|n\rangle. \quad (33)$$

It is then straightforward to relate the contribution of a resonance R with isospin $1/2$ to the interference γZ cross section entering Eq. (16) to its contribution to the electromagnetic cross section:

$$\langle p|J^{\mu}_{em}|R\rangle\langle R|J^{\mu}_{NC,V}|p\rangle = (1 - 4s^2\theta_W)\left|\langle R|J^{\mu}_{em}|p\rangle\right|^2 - \langle p|J^{\mu}_{em}|R\rangle\langle R|J^{\mu}_{em}|n\rangle. \quad (34)$$

Consequently, for each resonance, we define two ratios describing the relative strength of its contribution to the γZ-interference cross sections $\sigma^{\gamma Z,p}_{T(L),R}$ with respect to the purely electromagnetic ones $\sigma^{\gamma p}_{T(L),R}$ as

$$\xi^R_{Z/\gamma}(Q^2) \equiv \frac{\sigma^{\gamma Z,p}_{T,R}}{\sigma^{\gamma p}_{T,R}}, \qquad \zeta^R_{Z/\gamma}(Q^2) \equiv \frac{\sigma^{\gamma Z,p}_{L,R}}{\sigma^{\gamma p}_{L,R}}. \quad (35)$$

In the Appendix we discuss in detail the Q^2 dependence of these ratios, as well as the ratios of the longitudinal cross sections $\zeta^R_{Z/\gamma}$. Based on the discussion in the Appendix, we use the value

$$\xi^R_{Z/\gamma}(Q^2) = [1 - 4s^2\theta_W(0)] - y_R = \text{const}. \quad (36)$$

to rescale the contribution of a resonance R to both transverse and longitudinal cross section. Possible discrepancies (which, if known, are model dependent) from this rule are accounted for by assigning a conservative uncertainty to the ratios $\xi^R_{Z/\gamma}$.

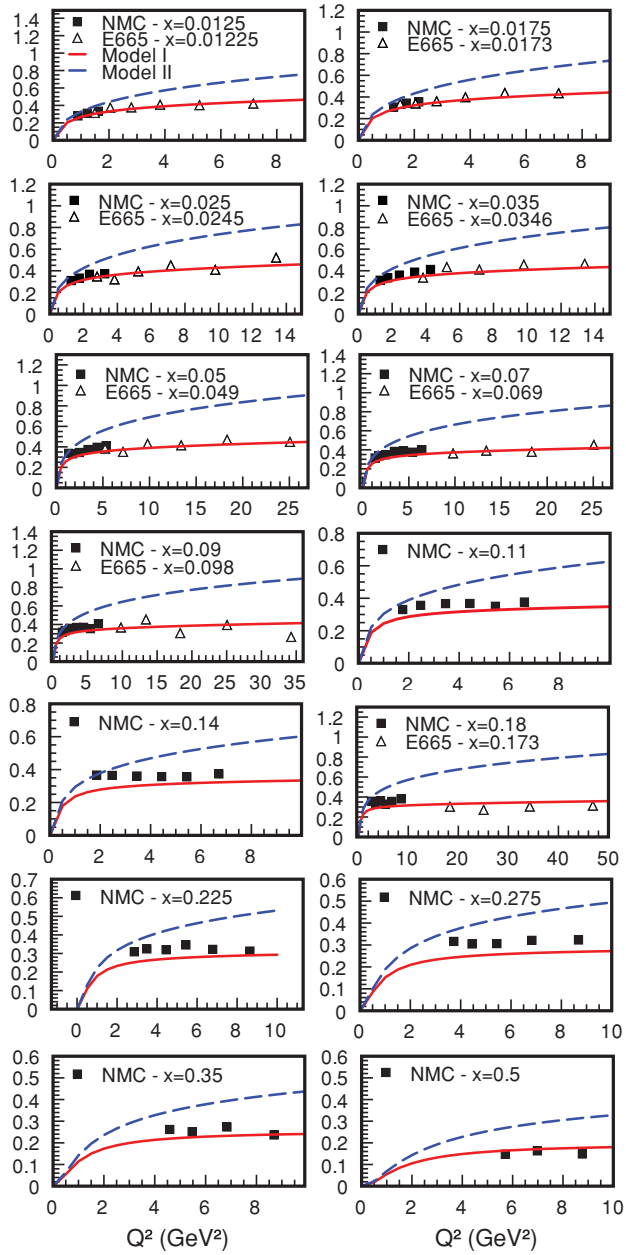

FIG. 11. (Color online) Comparison of the Q^2 dependence of the DIS structure function $F_2(x, Q^2)$ at fixed x and as a function of Q^2 in the GVD/CDP model of Ref. [37] (solid lines) and the naive GVD model of Ref. [39] (dashed lines) to the DIS data of the NMC Collaboration [31] and the E665 Collaboration [32], where the x-binning corresponds to that of NMC. The experimental errors are not shown.

TABLE III. Ratios y_R with respective uncertainties for seven resonances.

	$P_{33}(1232)$	$S_{11}(1535)$	$D_{13}(1520)$	$S_{11}(1665)$	$F_{15}(1680)$	$P_{11}(1440)$	$F_{37}(1950)$
y_R	$-1.0^{-0.1}_{+0.1}$	$-0.51^{-0.71}_{+0.35}$	$-0.77^{-0.125}_{+0.125}$	$-0.28^{-0.86}_{+0.45}$	$-0.27^{-0.12}_{+0.1}$	$-0.62^{-0.2}_{+0.19}$	-1^{-1}_{+1}

This is done by using the PDG values and respective errors for the transition helicity amplitudes. These PDG values represent an average over different data sets and different extraction procedures adopted in the various experiments. Consequently, they automatically include an enhanced error owing to model dependence of this extraction.

The first term in Eq. (36) is a constant that is model independent, arising from Eq. (34). This model independence reflects the cancellation of the proton-to-resonance transition matrix elements involving the e.m. currents. The second term in Eq. (36), y_R, is given by the ratio of combinations of neutron and proton transverse helicity amplitudes (we refer the reader to the Appendix for details). We summarize the values of y_R obtained using the PDG values for the helicity amplitudes with the respective errors in Table III. The lower and upper limits correspond to taking extreme values of the transition helicity amplitudes for the proton and neutron from Ref. [40].

For the $P_{33}(1232)$ resonance, we assign a conservative 10% error on its isospin structure. According to the PDG, this error should be precisely zero. However, the analyses of Refs. [38,42] return slightly different results for the $P_{33}(1232)$ excitation on the proton and the neutron, for both real and virtual photons. The discrepancy stays below relative 10% for $Q^2 \leqslant 1$ GeV^2, although this conclusion is definitely model dependent. This observation provides motivation for assigning a conservative 10% error to y_R for the $P_{33}(1232)$.

Similarly, for the $F_{37}(1950)$ resonance, the uncertainty is driven by the analyses of Refs. [38,42]. The fit of Ref. [38] for the proton returns a very mild monopole form factor, whereas the neutron data require a dipole form factor for the same resonance [42]. Also, the strength strongly depends on the form of the background, as found in our work (see Table II). This motivated us to assign a conservative 100% uncertainty owing to this resonance.

We note that for both S_{11} resonances listed in Table III the error bar exceeds 100%. This is mostly due to the quality of the extracted values for the neutron. It is also worth noting that the quark model expectations (see Table I of Ref. [16] for the isospin scaling factors within the quark model of Ref. [43]) are not too far from the central values quoted in Table III.

1. Uncertainty in isospin rotating the resonances

To summarize the results of the previous section, we propose to obtain the contribution of a resonance R to the γZ-interference cross sections $\sigma_{T,L}^{\gamma Z,R}$ by multiplying the purely electromagnetic cross sections $\sigma_{T,L}^{\gamma\gamma,R}$ with a scaling factor $\xi_{Z/\gamma}^R$ that is *independent of* W^2 *and* Q^2. Furthermore, to the precision required here, we rescale the transverse and longitudinal cross sections with the same factor. Each such factor contains two parts, as per Eq. (36): The first one is model independent, whereas the second one is obtained from the analysis of the proton and neutron electromagnetic data and involves model dependence and experimental uncertainties. The values of y_R are listed in Table III with the respective uncertainties. Correspondingly, for each resonance we simply obtain its contribution to the interference structure functions $F_{1,2}^{\gamma Z,R}$ from that to the electromagnetic structure functions $F_{1,2}^{\gamma\gamma,R}$ as

$$F_{1,2}^{\gamma Z,R}(W^2, Q^2) = \xi_{Z/\gamma}^R F_{1,2}^{\gamma\gamma,R}(W^2, Q^2). \tag{37}$$

To compute $\mathrm{Re}\,\Box_{\gamma Z_A}$, we use Eqs. (20) and (16) with the input from Eqs. (37) and (25). Finally, we use the parametrizations of the transverse and longitudinal electromagnetic cross sections from Model I and Model II and values of $\xi_{Z/\gamma}^R$ factors from Table III. The uncertainty on the contribution of each resonance is obtained according to the definition

$$\Delta F_{1,2}^{\gamma Z,R}(W^2, Q^2) = \Delta y_R F_{1,2}^{\gamma\gamma,R}(W^2, Q^2), \tag{38}$$

where Δy_R are the uncertainties quoted in Table III. Using the steps described above for the individual contributions of resonances to $\mathrm{Re}\,\Box_{\gamma Z_A}^R$, we can also compute the uncertainties $\Delta\left(\mathrm{Re}\,\Box_{\gamma Z_A}^R\right)$ associated with each such contribution. Because most resonances do not overlap, we treat all these uncertainties as independent; thus, we define

$$\Delta_R^{\mathrm{Full}}\mathrm{Re}\,\Box_{\gamma Z} = \sqrt{\sum_R \left|\Delta\left(\mathrm{Re}\,\Box_{\gamma Z_A}^R\right)\right|^2}. \tag{39}$$

C. Isospin rotation of the high-energy contribution

We need to employ a well-motivated model to describe the isospin dependence of the background contribution. One option is to employ the the VDM picture, incorporating the simple observation that the photon has the same quantum numbers as vector mesons (VMs). Therefore, it can fluctuate into ρ, ω, or ϕ that then scatter off the nucleon. This approach underlies the background in both Models I and II, so we proceed generally at first.

According to the VDM, the photon can be represented as a superposition of a few vector mesons,

$$|\gamma\rangle = \sum_{V=\rho,\omega,\phi} \frac{e}{f_V}|V\rangle, \tag{40}$$

with f_V the VM decay constant. Assuming this basis to be complete and orthogonal (no VM mixing), one can express the total photoabsorption cross section through a combination of total cross sections for vector meson-proton scattering,

$$\sigma_{\mathrm{tot}}(\gamma p) = \sum_V \frac{4\pi\alpha}{f_V^2}\sigma_{Vp}. \tag{41}$$

At high energies, the total cross section σ_{Vp} should be independent of the VM flavor and the above equation becomes simply a flavor decomposition of the electromagnetic total cross section, although this representation is of limited use because σ_{Vp} is unknown. Nevertheless, after trivial manipulations this picture leads to the VDM (Stodolsky) sum rule [44] that relates the total, real photoabsorption cross section to a sum of differential cross sections for photoproduction of vector mesons,

$$\sigma_{\rm tot}(\gamma p) = \sum_{V=\rho,\omega,\phi} \sqrt{16\pi \frac{4\pi\alpha}{f_V^2} \frac{d\sigma^{\gamma p\to Vp}}{dt}(t=0)}. \tag{42}$$

This sum rule is based on the assumptions of VDM and almost purely imaginary phase of scattering amplitudes at high energy.

In the naive GVD approach (Model II), this sum rule holds only approximately (HERA data, $\approx$80%) [45]. The missing strength can be attributed to the neglect of nondiagonal vector meson-nucleon scattering $Vp \to V'p$. One can then generalize the VDM by including such contributions by writing a dispersion relation over the vector meson masses. We denote this nondiagonal "continuum" contribution as "X" in the sum over vector mesons V.

Alternately, in the GVD/CDP approach (Model I), instead of hadronic VM states, the photon hadronic wave function (WF) is described in terms of perturbative $q\bar{q}$ states with $J = 1$. This $q\bar{q}$ pair forms a color dipole (CDP) that interacts with the target through gluon exchanges.

Both the naive GVD and GVD/CDP approaches are similar in the following instances: They consider the interaction of the hadronlike photon with the target (hadronic WF for naive GVD and perturbative $q\bar{q}$ for GVD/CDP), and the interaction of the hadronic states is independent of flavor (either VM or quark). This allows us to cast the ratio of inclusive virtual photon and γZ-interference cross sections in the following form:

$$\begin{aligned} \sigma_{\gamma^* p} &= \sum_{V=\rho^0,\omega,\phi,X} r_{\gamma^* V}(W^2, Q^2)\sigma_{Vp}, \\ \sigma_{\gamma^* Zp} &= \sum_{V=\rho^0,\omega,\phi,X} r_{\gamma^* ZV}(W^2, Q^2)\sigma_{Vp}, \end{aligned} \tag{43}$$

where "X" denotes the nondiagonal contribution.

According to the assumptions of both approaches, the flavor factors $r_{\gamma^* V}(W^2, Q^2)$ and $r_{\gamma^* ZV}(W^2, Q^2)$ only contain the information about the projectile (virtual photon or Z) and not about the target; this means that they cannot depend on the energy but only on Q^2 (the only Lorentz scalar that can be constructed from the γ four momentum) and the flavor of the VM state. However, if these flavor factors indeed depend on energy, this would signal the breakdown of the models and would be a source of an additional theory uncertainty. For completeness, we keep the W^2 dependence. The interference flavor factors $r_{\gamma^* ZV}$ obtain from the purely electromagnetic ones using the conservation of the vector current (CVC),

$$\begin{aligned} r_{\gamma^* Z\rho}(W^2, Q^2) &= \frac{g_V^{I=1}}{e_q^{I=1}} r_{\gamma^*\rho}(W^2, Q^2) \\ &= (2 - 4\sin^2\theta_W) r_{\gamma^*\rho}(W^2, Q^2), \\ r_{\gamma^* Z\omega}(W^2, Q^2) &= \frac{g_V^{I=0}}{e_q^{I=0}} r_{\gamma^*\omega}(W^2, Q^2) \\ &= -4\sin^2\theta_W r_{\gamma^*\omega}(W^2, Q^2), \\ r_{\gamma^* Z\phi}(W^2, Q^2) &= \frac{g_V^{s}}{e_q^{s}} r_{\gamma^*\phi}(W^2, Q^2) \\ &= (3 - 4\sin^2\theta_W) r_{\gamma^*\phi}(W^2, Q^2), \end{aligned} \tag{44}$$

for the light flavors.

With these definitions, we obtain our master formula for rescaling the background contribution:

$$\begin{aligned} \frac{\sigma_{T,L}^{\gamma^* p\to Zp}}{\sigma_{T,L}^{\gamma^* p\to\gamma^* p}} &= \frac{(2 - 4\sin^2\theta_W) r_{\gamma^* Z\rho}^{T,L}(W^2, Q^2) - 4\sin^2\theta_W r_{\omega}^{T,L}(W^2, Q^2) + (3 - 4\sin^2\theta_W) r_{\phi}^{T,L}(W^2, Q^2) + r_{\gamma^* ZX}^{T,L}(W^2, Q^2)}{r_{\gamma^*\rho}^{T,L}(W^2, Q^2) + r_{\gamma^*\omega}^{T,L}(W^2, Q^2) + r_{\gamma^*\phi}^{T,L}(W^2, Q^2) + r_{\gamma^* X}^{T,L}(W^2, Q^2)} \\ &= \frac{(2 - 4\sin^2\theta_W) - 4\sin^2\theta_W R_{\frac{\omega}{\rho}}^{T,L}(W^2, Q^2) + (3 - 4\sin^2\theta_W) R_{\frac{\phi}{\rho}}^{T,L}(W^2, Q^2) + \frac{r_{\gamma^* ZX}^{T,L}}{r_{\gamma^*\rho}^{T,L}}}{1 + R_{\frac{\omega}{\rho}}^{T,L}(W^2, Q^2) + R_{\frac{\phi}{\rho}}^{T,L}(W^2, Q^2) + R_{\frac{X}{\rho}}^{T,L}(W^2, Q^2)}. \end{aligned} \tag{45}$$

The ratios $R_{\frac{V}{\rho}}^{T,L}$ are defined as ratios of transverse (T) or longitudinal (L) vector meson (V) production cross sections:

$$R_{\frac{V}{\rho}}^{T,L} = \frac{\sigma_{T,L}^{\gamma^* p\to Vp}}{\sigma_{T,L}^{\gamma^* p\to\rho p}}. \tag{46}$$

The terms $\sim r_{\gamma^* X}^{T,L}$, $r_{\gamma^* ZX}^{T,L}$ account for the possible incompleteness of the VDM (or three light flavor) basis.

For the naive GVD model, $R_{\frac{V}{\rho}}^{T,L}$ are obtained from the experimentally measured constants f_V of the leptonic decay $V \to e^+e^-$. Additionally, the presence of the VM propagator leads to a prediction for the Q^2 dependence of each flavor channel $\sim\left(\frac{m_V^2}{m_V^2+Q^2}\right)^2$; thus, we have

$$R_{\frac{V}{\rho}}^{T} = R_{\frac{V}{\rho}}^{L} = \frac{\sigma^{\gamma^* p\to Vp}}{\sigma^{\gamma^* p\to\rho p}} = \frac{f_\rho^2}{f_V^2}\frac{m_V^4}{m_\rho^4}\left(\frac{m_\rho^2 + Q^2}{M_V^2 + Q^2}\right)^2, \tag{47}$$

with $V = \omega, \phi$. The remaining piece, $R^{T,L}_{\frac{X}{\rho}}$ is identified with the continuum (V-V' mixing) contribution. From the comparison of the left- and right-hand sides of the VDM sum rule [45] and supplementing this contribution with a simple Q^2 dependence to describe the virtual photoabsorption data at low and moderate Q^2, one obtains, for example, for the transverse ratio [39]

$$R^T_{\frac{C}{\rho}} = R_{\frac{C}{\rho}}(0)\frac{\left(1+Q^2/m_\rho^2\right)^2}{\left(1+Q^2/m_0^2\right)}, \tag{48}$$

with $R_{\frac{C}{\rho}}(0) = \frac{0.21}{0.67}$ and $m_0 \approx 1.5$ GeV. We note that because of the monopole Q^2 dependence of the continuum contribution, rather than dipole for the ρ^0, the impact of the continuum part increases with growing Q^2. The master formula of Eq. (45)–together with the model input of Eqs. (47) and (48) (see Ref. [39] for all the details of the model)–defines our prescription for the isospin rotation of the background contribution within the naive GVD model (Model II).

For pQCD-inspired models, such as the GVD/CDP used in Model I, the relative strength of the isospin (flavor) channels is directly related to the quark electric charges and is independent of energy and Q^2:

$$\begin{aligned}\sigma^{\gamma\to\rho} &: \sigma^{\gamma\to\omega} : \sigma^{\gamma\to\phi} : \sigma^{\gamma\to J/\psi} \\ &= 1 : \frac{(q^{I=0})^2}{(q^{I=1})^2} : \frac{(q^s)^2}{(q^{I=1})^2} : \frac{(q^c)^2}{(q^{I=1})^2} = 1 : \frac{1}{9} : \frac{2}{9} : \frac{8}{9}.\end{aligned} \tag{49}$$

One possible way is to identify the X state in the master formula with the $c\bar{c}$ state, that is, J/ψ. In that case, the X contribution in the numerator of Eq. (45) is given according to the SM

$$\frac{r^{T,L}_{\gamma^* ZX}}{r^{T,L}_{\gamma^*\rho}} = \frac{3-8\sin^2\theta_W}{2} R^{T,L}_{\frac{J/\psi}{\rho}}. \tag{50}$$

The choice of identifying X with J/ψ is justified in HERA kinematics but is probably less convincing at lower energies and low Q^2. Moreover, the choice $X = J/\psi$ and the relative strength of different contributions according to Eq. (49) corresponds to the VDM sum rule being saturated to only 60%, rather than the measured 80%, suggesting that it is not very realistic.

Either way, for the rescaling of the background contribution in the GVD/CDP model (Model I), Eqs. (45) and (49) simply combine to a constant factor. Its value when using only the three light flavors amounts to

$$\left[\frac{\sigma^{\gamma^* p\to Zp}}{\sigma^{\gamma^* p\to\gamma^* p}}\right]^{\text{Model I}}_{u,d,s} = 2 - 4\sin^2\theta_W \approx 1.05. \tag{51}$$

However, when including the charm contribution, one obtains

$$\left[\frac{\sigma^{\gamma^* p\to Zp}}{\sigma^{\gamma^* p\to\gamma^* p}}\right]^{\text{Model I}}_{u,d,s,c} = \frac{9}{5} - 4\sin^2\theta_W \approx 0.85. \tag{52}$$

For comparison, a typical value of this ratio within the naive GVD Model II (we quote its value at $Q^2 = 0$ for definiteness: in Model II it is Q^2 dependent, although mildly) is

$$\left[\frac{\sigma^{\gamma^* p\to Zp}}{\sigma^{\gamma^* p\to\gamma^* p}}\right]^{\text{Model II}}_{\rho,\omega,\phi} \approx 1.92 - 4\sin^2\theta_W \approx 0.97, \tag{53}$$

and a very similar number when including the continuum and assuming its size for the γZ cross section to be equal to that for the purely electromagnetic case. However, any such estimate bears at least 20% uncertainty owing to the incompleteness of the naive VDM basis and owing to the unknown flavor structure of the continuum contribution.

To illustrate the difference in the Q^2 dependence of the total cross section as calculated in Model I and Model II, we define the following two ratios:

$$\begin{aligned}R_{\gamma\gamma}(W^2, Q^2) &= \frac{\left[\sigma_T^{\gamma^* p\to\gamma^* p} + \sigma_L^{\gamma^* p\to\gamma^* p}\right]^{\text{Model I}}}{\left[\sigma_T^{\gamma^* p\to\gamma^* p} + \sigma_L^{\gamma^* p\to\gamma^* p}\right]^{\text{Model II}}}, \\ R_{\gamma Z}(W^2, Q^2) &= \frac{\left[\sigma_T^{\gamma^* p\to Zp} + \sigma_L^{\gamma^* p\to Zp}\right]^{\text{Model I}}}{\left[\sigma_T^{\gamma^* p\to Zp} + \sigma_L^{\gamma^* p\to Zp}\right]^{\text{Model II}}},\end{aligned} \tag{54}$$

where we suppressed the arguments of the cross sections for compactness. In Fig. 12 we display the Q^2 dependence of $R_{\gamma\gamma}$ and $R_{\gamma Z}$ at two values of W^2. The ratios show very mild W^2 dependence, in accord with general assumptions used in VDM and GVD/CDP models. The Q^2 dependence shows slight oscillations (at the level of 3%) at $Q^2 \lesssim 2$ GeV^2; at higher values of Q^2 both ratios decrease monotonically, as a result of the naive VDM model (Model II) overshooting

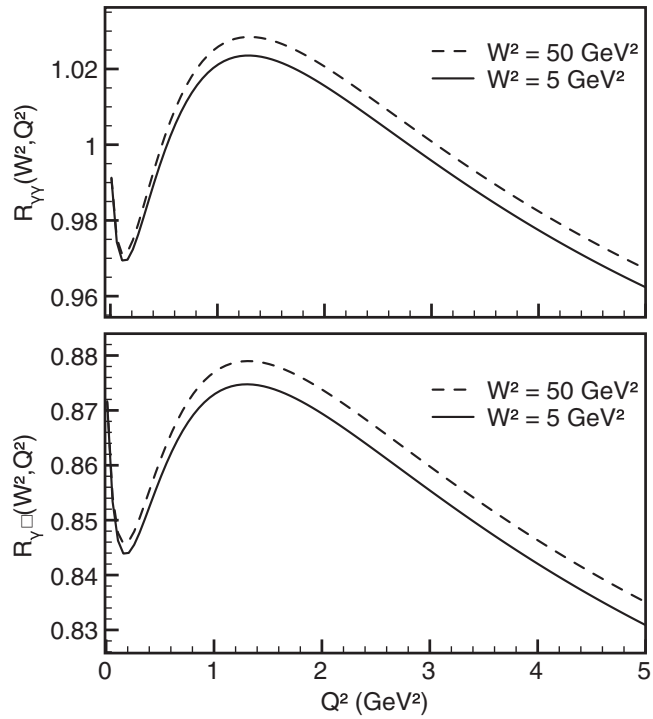

FIG. 12. Ratios $R_{\gamma\gamma}(W^2, Q^2)$ (top) and $R_{\gamma Z}(W^2, Q^2)$ (bottom) are shown as function of Q^2 at $W^2 = 5$ GeV^2 (solid lines) and at $W^2 = 50$ GeV^2 (dashed lines). See text for further details.

high-Q^2 data significantly, while GVD/CDP Model I describes data in a wide kinematical range.

1. Uncertainty in isospin rotating the background

We wrote our master formula in terms of ratios of meson production cross sections, rather than cross sections themselves. These ratios were recently measured at HERA. The predictions of Eqs. (47) and (49) are confronted with the experimental data of Ref. [46] at high energies and for Q^2 that ranged from zero to several GeV^2 in Fig. 13. To estimate uncertainties in isospin rotation of Models I and II, we directly compare the model predictions of the isospin ratios to the HERA data. The common feature of the two models is that these ratios are W^2 independent. Furthermore, Model I predicts them to be Q^2 independent, too. Instead, Model II (naive GVD) predicts the Q^2 running of these ratios. In both cases, we assume that the uncertainty in isospin scaling the $I = 1$ channel (i.e., the ρ^0) is zero. For each flavor channel, we define the uncertainty as the discrepancy

$$\Delta\frac{\sigma^{\gamma\to V}}{\sigma^{\gamma\to\rho}}(Q^2) = \left(\frac{\sigma^{\gamma\to V}}{\sigma^{\gamma\to\rho}}\right)^{\text{Model}} - \left(\frac{\sigma^{\gamma\to V}}{\sigma^{\gamma\to\rho}}\right)^{\text{exp}}, \qquad (55)$$

with $V = \rho, \omega$ for VDM and $V = \rho, \omega, (J/\psi)$ for pQCD. Additionally, for VDM we assign a 100% uncertainty to the continuum contribution whose flavor content is not defined in the naive GVD approach. Similarly, for GVD/CDP model we assign a conservative 100% uncertainty to the $c\bar{c}$ contribution,

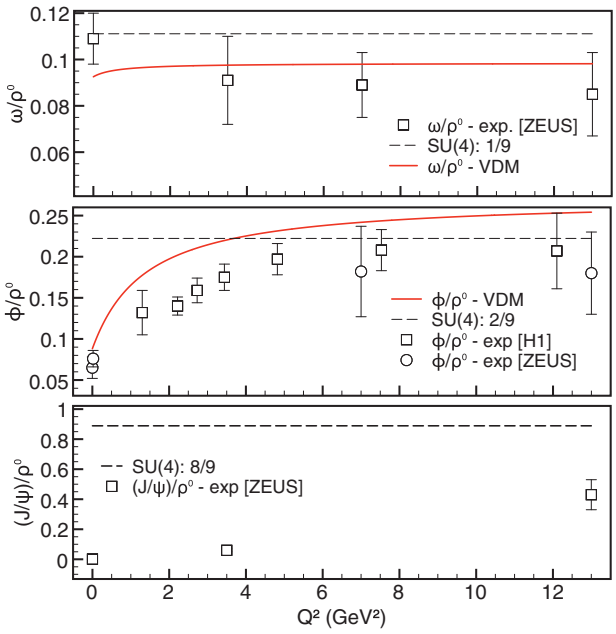

FIG. 13. (Color online) Experimental data for ratios of total cross sections for elastic vector meson electroproduction in comparison with the naive VDM (solid lines) and perturbative SU(4) (dashed lines) predictions.

in view of an unsatisfactory description of the data for $(J/\psi)/\rho$ by the SU(4) prediction.

Arriving at the estimate of the total uncertainty owing to the isospin structure of the background requires following steps. For Models I and II, we insert the uncertainties defined in Eq. (55) and below for each flavor V into the master formula Eq. (45). Subsequently, we use the relation of Eq. (25) and obtain the total uncertainty of the interference structure functions, $\Delta F_{1,2}^{\gamma Z}$. We evaluate the imaginary part of the dispersion correction of Eq. (16) with $\Delta F_{1,2}^{\gamma Z}$. The final step involves evaluating the dispersion integral thereof [Eq. (20)]. These steps give us the uncertainties owing to the isospin structure of the background within Model I and Model II. To be conservative, we choose the larger of the two as our estimate of the nonresonant model uncertainty.

Anticipating the discussion in the next section, we note that the overall uncertainty is dominated by the continuum contribution ("X") within the naive GVD model. The only significant assumption about the continuum contribution here is that its size (relative to diagonal vector meson contributions) is energy independent, and we take it from the data at very high W^2. Until now, the only dedicated study of the VDM sum rule was performed at $W \geqslant 70$ GeV at HERA–far from the kinematic region that dominates the dispersion integral for $\Box_{\gamma Z}$. It is not *a priori* clear that the decomposition of the virtual photon into the VM basis works any differently for 5-GeV photons than for 80-GeV photons.

As part of a program of future measurements to constrain the uncertainties in the dispersion correction, it would be useful to have direct data on this sum rule at lower energies: $2 \leqslant W \leqslant 10$ GeV. In case that new data on the VDM sum rule at these energies become available, it will then be straightforward to include additional W-dependent form factors in Eq. (45). Data on the virtual vector meson photoproduction cross sections in this kinematic regime could also provide additional important constraints. Together with direct measurements of the inelastic PV asymmetries at these kinematics, such measurements could, in principle, lead to a significant reduction in the quoted theoretical error bar.

V. RESULTS FOR RE$\Box_{\gamma Z}$

We are now in the position to present results for $\Box_{\gamma Z}$ in the forward direction using the sum rule of Eqs. (16) and (20), the Models I and II for the electromagnetic cross sections along with the isospin considerations provided in the previous sections.

We display the sum of resonance and background in Fig. 14.

In Fig. 15, we display the contributions of various kinematic regions to Re $\Box_{\gamma Z}$. The top panel of Fig. 15 evidences that the resonance contribution is dominated by values of $Q^2 \leqslant 1$ GeV^2, whereas for the total correction, values of Q^2 up to 3 GeV^2 have to be taken to saturate the dispersion correction to ≈90%. The bottom panel of that figure demonstrates that values of W^2 up to 25 GeV^2 have to be included under the integration to saturate the dispersion correction Re $\Box_{\gamma Z}$. The data from the resonance region $W^2 \leqslant 5$ GeV^2 (resonance

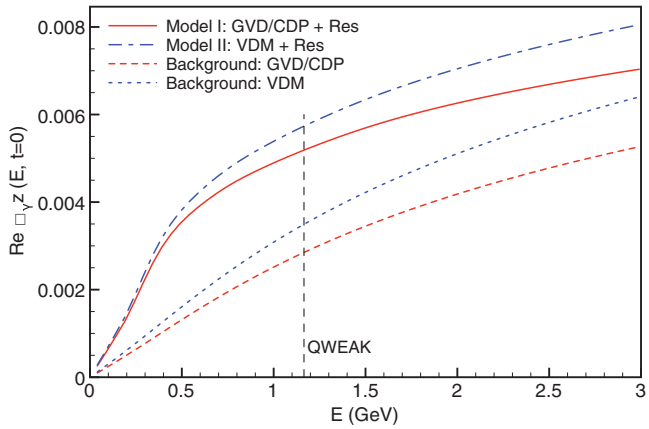

FIG. 14. (Color online) Sum of resonance and background contributions to Re $\Box_{\gamma Z}$ for Models I and II as indicated in the legend of the plot.

plus background) only contribute about 65% of the total. The notation $Q^2 \leqslant Q_A^2$ and $W^2 \leqslant W_B^2$ refers to evaluating the double integral for Im $\Box_{\gamma Z}$ in Eq. (16) only over those values of Q^2 (W^2) that lie below Q_A^2 (W_B^2), respectively. After that, the dispersion integral of Eq. (20) is evaluated without further modifications.

In Table IV, we display the background contribution as calculated in Models I and II for the Q-Weak kinematics. It can be seen that the background represents both the largest contribution and the source of the largest uncertainty. Most notably, within the naive GVD approach (Model II), it is completely dominated by the continuum contribution whose isospin structure is undetermined. In the pQCD approach (Model I), a contribution similar in strength is assigned to the $c\bar{c}$ state. However, because in this case we know exactly how the weak boson couples to c quarks, the uncertainty is about half the size of that for Model II. This 50% reduction is simply because of to the fact that $g_V^c \approx \frac{1}{3} = \frac{1}{2} e_c$.

The individual resonance contributions are displayed in Table V. It can be seen that the overall uncertainty in the resonance contribution is dominated by the uncertainty in two contributions, namely $S_{11}(1535)$ and $F_{37}(1950)$. The former, in turn, is dominated by the uncertainty in the neutron transition helicity amplitude. The heavy resonance state is not well-determined and should be studied in greater detail to decrease the respective uncertainty for the dispersion correction.

According to the discussion in the previous section, we plot the result for Re $\Box_{\gamma Z}$ and display the error bar for this calculation in Fig. 16. For the central value, we take the average of Model I and Model II and use the difference between this central value and either of Model I or II as the

TABLE IV. Background contribution to the dispersion correction to the weak charge of the proton Re$\Box_{\gamma Z}$ at the Q-Weak energy $E_{\rm lab} = 1.165$ GeV. Results for Model I and Model II are shown.

	Background
Model I	$(2.85 \pm 0.85) \times 10^{-3}$
Model II	$(3.49 \pm 1.92) \times 10^{-3}$

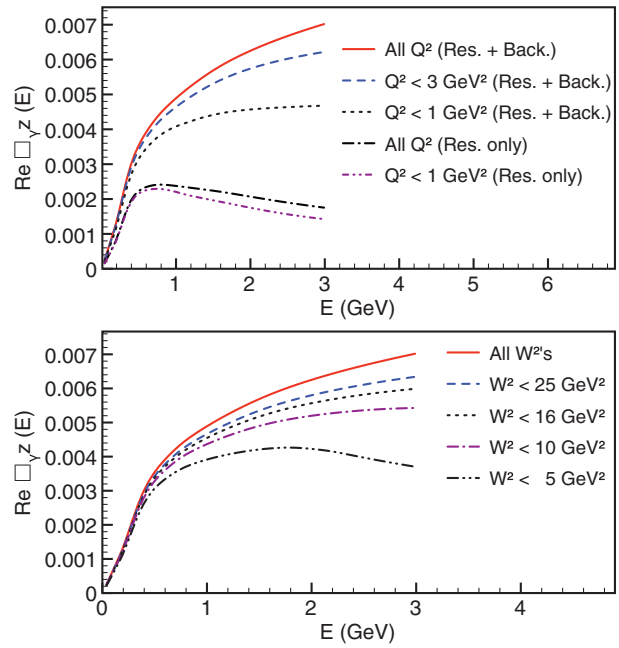

FIG. 15. (Color online) Contributions of different kinematic regions to $\Box_{\gamma Z}$ for Model I. In the top panel, contributions from various Q^2 ranges are shown: solid curve (full result), dashed line ($Q^2 < 3$ GeV^2 for resonance + background), dotted line ($Q^2 < 1$ GeV^2 for resonance + background). For comparison, in the top panel we display result of integration of the resonance contribution to $\Box_{\gamma Z}$ over all values of Q^2 (dash-dotted curve) and $Q^2 < 1$ GeV^2 (dash-double-dotted curve). In the bottom panel, contributions to $\Box_{\gamma Z}$ are shown that come from $W^2 \leqslant 5$ GeV^2 (dash-double-dotted curve), $W^2 \leqslant 10$ GeV^2 (dash-dotted curve), $W^2 \leqslant 16$ GeV^2 (dotted curve), $W^2 \leqslant 25$ GeV^2 (dashed curve), and full result (solid curve).

uncertainty owing to modeling the e.m. data. For the isospin rotation-related uncertainty, we calculate the error within each model as discussed before, and quote the larger of the two. We summarize this section by quoting the result of the forward sum rule evaluated within two models as follows:

$$\mathrm{Re}\,\Box_{\gamma Z}(E = 1.165\mathrm{GeV}, t = 0) = \big[5.46 \pm 0.27(\mathrm{mod.\ avg.}) \pm 1.92(\mathrm{backgr.})^{+0.59}_{-0.50}(\mathrm{res.})\big] \times 10^{-3}. \quad (56)$$

The first uncertainty corresponds to averaging over the two models, the second to the uncertainty in isospin rotating the background, and the third to isospin rotating the resonance contributions. A possibility of measuring the proton's weak charge at Mainz at a lower energy $E_{\rm lab} = 180$ MeV is under consideration presently [47], and we quote our prediction for the dispersion γZ correction and the respective uncertainty for that energy,

$$\mathrm{Re}\,\Box_{\gamma Z}(E = 0.180\,\mathrm{GeV}, t = 0) = \big[1.32 \pm 0.05\,(\mathrm{mod.\ avg.}) \pm 0.27\,(\mathrm{backgr.})^{+0.11}_{-0.08}\,(\mathrm{res.})\big] \times 10^{-3}\,. \quad (57)$$

We see that the total uncertainty in Re$\Box_{\gamma Z}$ is about six times smaller at $E_{\rm lab} = 180$ MeV than at $E_{\rm lab} = 1.165$ GeV.

TABLE V. Resonance contributions to the dispersion correction to the weak charge of the proton $\mathrm{Re}\Box_{\gamma Z}$ at the Q-Weak energy $E_{\mathrm{lab}} = 1.165$ GeV, in units of 10^{-3}. For each contribution, we indicate the uncertainty discussed in the text. Results for Model I and Model II are shown.

	$P_{33}(1232)$	$S_{11}(1535)$	$D_{13}(1520)$	$S_{11}(1665)$	$F_{15}(1680)$	$P_{11}(1440)$	$F_{37}(1950)$	$\sum$ Res.
Model I ($\times 10^{-3}$)	(1.21 ± 0.12)	$(0.28^{+0.34}_{-0.17})$	(0.18 ± 0.03)	$(0.06^{+0.14}_{-0.06})$	$(0.04^{+0.013}_{-0.011})$	(0.09 ± 0.03)	(0.48 ± 0.44)	$(2.34^{+0.59}_{-0.50})$
Model II ($\times 10^{-3}$)	(1.23 ± 0.12)	$(0.29^{+0.34}_{-0.17})$	(0.18 ± 0.03)	$(0.06^{+0.14}_{-0.06})$	$(0.04^{+0.013}_{-0.011})$	(0.06 ± 0.02)	(0.40 ± 0.36)	$(2.24^{+0.53}_{-0.43})$

VI. ADDITIONAL t-DEPENDENCE OF DISPERSION CORRECTIONS

In the previous section, we provided an educated estimate for Re $\Box_{\gamma Z}$ in the exact forward direction. However, real experiments are carried out at finite momentum transfer t, in particular $|t| = 0.03$ GeV^2 for the kinematics of the Q-Weak experiment. To extrapolate the forward sum rule to nonzero momentum transfer, we employ the phenomenological model that was successfully used for the beam normal spin (Mott) asymmetry in elastic ep scattering [48–50]. This model is inspired by (i) experimental data on the Compton differential cross section at small t and high energy, and (ii) the assumption of the predominantly imaginary phase of the Compton amplitude at high energies (as for the Pomeron).

The data exhibit an exponential t dependence,

$$\frac{d\sigma}{dt} = \left(\frac{d\sigma}{dt}\right)_{t=0} e^{-B|t|}, \tag{58}$$

with the slope parameter $B = 7 \pm 1$ GeV^{-2} [51]. The differential cross section is related to the Compton amplitude squared, whereas the total cross section—through the optical theorem—is related to the imaginary part of the Compton amplitude. Naively, then, one might expect the t dependence of the total cross section near the forward scattering limit to be close to half as rapid as that of the differential cross section. Based on this ansatz, Ref. [48] proposed parameterizing the t dependence of the slightly off-forward total cross section as

$$\sigma_{\mathrm{tot}}(t) \approx \sigma_{\mathrm{tot}}(t=0)\, e^{-\frac{B|t|}{2}}. \tag{59}$$

This parametrization becomes precise at very high energies where the cross section is Pomeron-dominated. We will follow a similar parametrization here.

This intrinsic t dependence of the γZ-box contribution should be combined with the $\gamma\gamma$-box contribution that becomes nonzero when going to finite t. We found the effect of the dispersive contributions to $\Box_{\gamma\gamma}$ on A^{PV} to be negligibly small, of order below 0.1% at the Q-Weak kinematics at $-t = 0.03$ GeV^2. The reason for this smallness is due to an explicit t suppression of $\Box_{\gamma\gamma}$ with respect to the tree-level PC amplitude. Using the same approach, we obtain for the t dependence of the dispersion correction

$$\Box_{\gamma Z}(E,t) = \Box_{\gamma Z}(E,0)\frac{\exp(-B|t|/2)}{F_1^{\gamma p}(t)}, \tag{60}$$

according to the definition of $\Box_{\gamma Z}$ as the ratio of the γZ-box contribution to the PV amplitude $f_4(E,t)$ to the elastic proton electromagnetic form factor $F_1^{\gamma p}(t)$.

In Fig. 17, we display the t dependence of the combined dispersion correction for small values of the elastic momentum transfer. It can be seen that one can expect that at $|t| = 0.03$ GeV^2, the dispersion correction decreases by only about 2% relative to its value at $t = 0$, and the same is valid for the uncertainty in calculating this correction. We emphasize, however, that the model for the t dependence is derived from high-energy Compton data, and it is not necessarily applicable to the resonance contributions. Thus, our estimate of the effect of the t dependence should be considered as an exploratory investigation. Having this caveat in mind and taking into account this t dependence, we obtain our final result for the dispersion γZ correction at the kinematics of the Q-Weak experiment:

$$\begin{aligned}&\mathrm{Re}\Box_{\gamma Z_A}(E = 1.165\,\mathrm{GeV}, t = -0.03\,\mathrm{GeV}^2)\\ &\quad = \left[5.39 \pm 0.27\,(\mathrm{mod.\ avg.}) \pm 1.88\,(\mathrm{backgr.})^{+0.58}_{-0.49}\,(\mathrm{res.})\right.\\ &\qquad \left. \pm 0.07\,(t-\mathrm{dep.})\right] \times 10^{-3}.\end{aligned} \tag{61}$$

To assess the relative impact of the energy-dependent contribution from $\Box_{\gamma Z_A}$ we first quote the result from Refs. [5,7] for the weak charge, as defined in Eq. (2):

$$Q_W^p = 0.0713 \pm 0.0008. \tag{62}$$

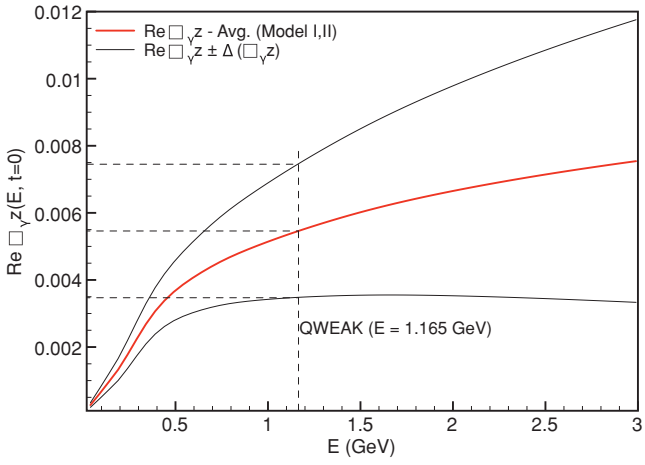

FIG. 16. (Color online) Full result for $\mathrm{Re}\Box_{\gamma Z}$ with the theoretical error bar.

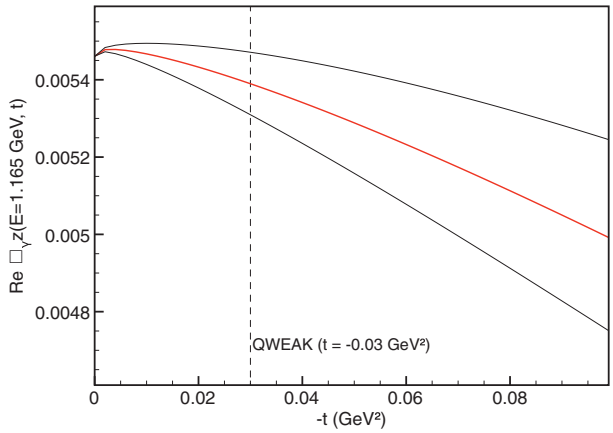

FIG. 17. (Color online) The dependence of the combined dispersion correction to Q_W^p on the elastic momentum transfer t. The central value is shown in grey (red online); the thin black lines indicate the uncertainty.

Compared to this prediction, the relative effect of the $\Box_{\gamma Z_A}$ contribution at the kinematics of the Q-Weak experiment is

$$\frac{\mathrm{Re}\Box_{\gamma Z_A}}{Q_W^p} = (7.6 \pm 2.8)\%. \tag{63}$$

Because this contribution was initially neglected in the analysis of radiative corrections for the Q-Weak experiment, the final theory prediction and the respective uncertainty have to be corrected to include it. Treating all the individual uncertainties quoted above as independent, we obtain

$$\lim_{t\to 0}\frac{W^{\mathrm{PV}}}{W^{\mathrm{EM}}} = Q_W^p + \Box_{\gamma Z_A} = (0.0767 \pm 0.0008 \pm 0.0020_{\gamma Z})\,. \tag{64}$$

As discussed in Refs. [5,7], the first error includes a conservative $\sim$1% error associated with $C_{\gamma Z}$ that appears in the prediction for Q_W^p. The additional uncertainty associated with the energy-dependent contribution from $\Box_{\gamma Z_A}$ is almost entirely due to the uncertainty in the isospin structure of the background. The latter, in turn, is largely dominated (70%) by the uncertainty owing to the "continuum" contribution that does not have well-defined isospin content.

To recollect, the continuum contribution that arises in both the naive GVD and GVD/CDP frameworks is a measure of the incompleteness of the vector meson basis for the energetic photon. Its value at the real photon point is obtained from the direct comparison of the VDM sum rule with the experimental photoproduction cross sections where one finds roughly a 20% deficit in the naive GVD approach. Departing from the real photon point, one employs phenomenological models for the Q^2 dependence for this contribution, such that in this way the generalized VDM description fits the virtual photoabsorption data at moderate Q^2. It turns out that above $Q^2 = 2\,\mathrm{GeV}^2$, the continuum contribution becomes dominant.

Strictly speaking, these observations only apply at high energies, as the VDM sum rule measurement at HERA was performed at $W = 82$ GeV. In absence of an independent evaluation at lower energies, we are forced to extrapolate this isospin decomposition down to lower energies. While this extrapolation is in line with the general assumptions of the VDM, there is no guarantee that the isospin decomposition of the photon wave function is energy independent. To illustrate where the high-energy assumptions may break down, we note that one of the purely high-energy scattering assumptions in the derivation of the VDM sum rule is the neglect of the real part of the forward Compton amplitude with respect to the imaginary part. While this holds for the Pomeron—whose phase is almost purely imaginary—Reggeon exchanges contribute to both real and imaginary parts. The main contribution to $\mathrm{Re}\Box_{\gamma Z}$ comes from energies of $W \lesssim 5$ GeV, where the Reggeon contribution dominates. Thus, a reevaluation of the VDM sum rule at JLab energies will likely help to reduce the theory uncertainty on the $\mathrm{Re}\Box_{\gamma Z}$ calculation.

VII. COMPARISON TO RELATED WORKS ON DISPERSION γZ CORRECTION

In this section, we briefly outline the main improvements achieved in this article with respect to our previous work, as well as the recent work carried out by other groups. In Ref. [11], the forward dispersion relation for $\Box_{\gamma Z}$ was derived and evaluated with the result of $\mathrm{Re}\Box_{\gamma Z} \approx 0.003$. However, that study used an oversimplified model of virtual photoabsorption and for the sake of simplicity assumed that $F_{1,2}^{\gamma Z} = F_{1,2}^{\gamma\gamma}$. These assumptions did not allow for a realistic study of uncertainty of that result.

In Ref. [16], we improved on these two points: We employed a phenomenological model of Bosted and Christy that fits virtual photoabsorption data over a large kinematic range, considered the isospin structure of each contribution, and discussed the possible ways to estimate uncertainty on this calculation. Although in Ref. [16] we were able to develop the general method that we use in this paper, no robust theory error bar was obtained.

Sibirtsev *et al.* in Ref. [15] rechecked the findings of Ref. [11]. That group carefully rederived the sum rule pointing out two errors in Ref. [11], which have been corrected here. Furthermore, the authors of Ref. [15] proposed a model of the virtual photoabsorption that was directly fit to the experimental data. This allowed them to obtain an estimate for the uncertainty in the dispersive calculation of $\Box_{\gamma Z}$ from the error bar of the fit. To obtain the interference structure functions $F_{1,2}^{\gamma Z}$ from the purely electromagnetic ones $F_{1,2}^{\gamma\gamma}$, the authors of Ref. [15] relied on isovector dominance in the resonance region. For the background, they employed a simple scaling prescription for the background

$$\frac{F_2^{\gamma Z}}{F_2^{\gamma\gamma}} = \left[\frac{F_2^{\gamma Z}}{F_2^{\gamma\gamma}}\right]^{\mathrm{DIS}}, \tag{65}$$

extrapolating the isospin structure from the DIS region to low energies. Reference [15] confirmed that the dispersion correction is sizable, obtaining the value quoted in Table I, where the error bar is attributable solely to fitting the electromagnetic data. The uncertainty on the isospin rotation of the electromagnetic data was not included. Correspondingly,

the error bar quoted in Ref. [15] only contains one part of the total theoretical uncertainty in evaluating $\mathrm{Re}\Box_{\gamma Z}$.

Rislow and Carlson subsequently performed another computation of the dispersive contribution to $\Box_{\gamma Z_A}$ [17]. These authors again confirmed the derivation of the sum rule and reevaluated it obtaining the somewhat larger result quoted in Table I. This was achieved by using a different model for the resonances (the same as used in our present work) that allows for a better fit of electromagnetic data. The central value of $\mathrm{Re}\Box_{\gamma Z}$ is very close to our estimate in forward direction [see Eq. (56)]. The background was taken in a phenomenological form and continued into the DIS region. The authors discussed in some detail the procedure of isospin-rotating the resonance contributions using the constituent quark model. For the background, Ref. [17] follows to a large extent the isovector dominance picture with a perturbation on top of that that provides an estimate of the uncertainty.

Both Refs. [15,17] argue that the uncertainty on the dispersive calculation of $\mathrm{Re}\Box_{\gamma Z}$ is well under control and can be easily accommodated within the error budget of the Q-Weak. However, because they do not provide a model-independent analysis of the isospin structure, we believe that the estimates of the error bars obtained in those two works is unlikely to be complete.

In this paper, we believe we have developed the most robust and model-independent estimate to date of the absolute size and the uncertainty of the dispersion γZ correction to A_{PV} in the forward limit. We used the most recent fit to resonance data, supplemented by two different models of the background. We demonstrated that the two models used in this work indeed provide a good description of the experimental data in a very wide kinematic range of two variables W, Q^2.

For the $I = 1/2$ resonances, we employed an isospin rotation that is reminiscent of that for the elastic electroweak form factors. This allows one to unambiguously relate the ratio of interference γZ and the electromagnetic cross sections to combinations of transition helicity amplitudes for the photoexcitation of a given resonance on the proton and the neutron. We used the most recent values and uncertainties for the latter from PDG [40]. The main sources of the uncertainty for the $I = 1/2$ resonances is the neutron transition helicity amplitude of $S_{11}(1535)$, where a more precise extraction of the transition helicity amplitude on the neutron would be needed. For the $I = 3/2$ resonances, the isospin rotation is straightforward. However, we assigned a 100% uncertainty to the contribution of the heavy resonance state that lies close to $F_{37}(1950)$ but cannot be reliably identified with the latter and whose isospin structure is, therefore, uncertain.

For the background we utilized two models based on the framework of vector meson dominance (VDM) that provides a prescription for the isospin decomposition of total photoabsorption at high energies. The VDM sum rule states an equality between the total photoabsorption and differential cross sections for forward vector meson production. This sum rule has been tested experimentally, albeit only at very high energies. The precision to which this sum rule holds provides us with one handle for assessing for the robustness of our isospin decomposition of the electromagnetic data. To investigate the model dependence, we use two different models that obey the general requirements of the VDM but originate from two kinematically distinct regimes: Model I is a pQCD CDP model (what we have called the GVD/CDP approach) that is continued down to the real photon point by employing phenomenological input [37]. Model II is a "naive" generalization of VDM quoted in Ref. [39]. The two models lead to similar numerical results, but within each model the estimate of uncertainties is different. The largest contribution to our quoted theoretical uncertainty arises from lack of knowledge of the isospin structure of the terms in these models that are not uniquely associated with any one of the three lightest vector mesons. To be conservative, we have chosen the largest of the corresponding uncertainties from the two models.

Finally, we considered a phenomenological model for the intrinsic t dependence to extrapolate the forward sum rule to the experimental kinematics. We find that the effect of such extrapolation is not significant. However, we consider this approach to be exploratory, and an additional uncertainty on t dependence may have to be taken into account.

To reduce the uncertainty associated with $\Box_{\gamma Z}$ to a level below 2%, there exist a number of avenues that could be pursued. The most direct would be to perform measurements of the inelastic PV asymmetries in the kinematic region that dominates the dispersion integral: $W < 5$ GeV and $Q^2 \lesssim 3$ GeV^2. Doing so would provide information on the electroweak structure functions $F_{1,2}^{\gamma Z}$ that enter the dispersion integral for $\Box_{\gamma Z}$, thereby mitigating the need for a model with which to carry out the isospin rotation. Additional constraints could be obtained by experimentally testing the VDM sum rule at the lower energies relevant to the aforementioned kinematics; by performing precise measurements of the electromagnetic neutron-to-resonance transition cross sections, thereby yielding the corresponding helicity amplitudes–particularly for the $S_{11}(1535)$; and by identifying the isospin of the $F_{37}(1950)$ resonance.

An alternate strategy would be to perform a measurement of A_{PV} at lower energy, given that the magnitude of, and uncertainty in, $\Box_{\gamma Z}$ decrease monotonically with decreasing energy, as indicated in Fig. 16 and Eq. (57). From the standpoint of probing physics beyond the Standard Model, a measurements of atomic PV observables for different isotopes may also be interesting. The largest atomic theory uncertainties cancel from ratios of these observables [52], and the leading sensitivity to new physics is dominated by the effects on the proton weak charge [3]. To the extent that uncertainties in the neutron distributions can be constrained (e.g., through measurements of the elastic PV asymmetry for heavy nuclei), "isotope ratio" experiments may provide a cross-check on any inferences about new physics derived from the Q-Weak measurement. Given the experimental and theoretical challenges involved in each of these efforts, an ideal program may entail a combination of the aforementioned measurements.

ACKNOWLEDGMENTS

Authors are grateful to W. Melnitchouk and C. Carlson for useful discussions and comments. This work was supported in

part by US DOE Contract No. DE-FG02-87ER40365 and NSF Grant No. Phy-0854805 (C.J.H. and M.G.) and by US DOE Contract No. DE-FG02-08ER41531(M.J.R-M). M.J.R.M. also gratefully acknowledges support from the Wisconsin Alumni Research Foundation and the Aspen Center for Physics, where part of this work was carried out.

APPENDIX: ISOSPIN ROTATION OF THE RESONANCE CONTRIBUTIONS

In Standard Model, the Z and γ couplings to the quarks are related by an isospin rotation,

$$\begin{aligned} J^{\mu}_{em} &= q^{I=0} J^{\mu}_{I=0} + q^{I=1} J^{\mu}_{I=1} + q^{s} J^{\mu}_{s}, \\ J^{\mu}_{NC_V} &= g_V^{I=0} J^{\mu}_{I=0} + g_V^{I=1} J^{\mu}_{I=1} + g_V^{s} J^{\mu}_{s}, \end{aligned} \tag{A1}$$

with

$$\begin{aligned} J^{\mu}_{I=0} &= \frac{1}{\sqrt{2}}(\bar{u}\gamma^{\mu}u + \bar{d}\gamma^{\mu}d), \\ J^{\mu}_{I=1} &= \frac{1}{\sqrt{2}}(\bar{u}\gamma^{\mu}u - \bar{d}\gamma^{\mu}d), \\ J^{\mu}_{s} &= \bar{s}\gamma^{\mu}s. \end{aligned} \tag{A2}$$

The e.m. charges are given by $q^{I=0} = \frac{1}{3\sqrt{2}}$, $q^{I=1} = \frac{1}{\sqrt{2}}$, $q^{s} = -\frac{1}{3}$, and the weak charges are $g_V^{I=0} = -\frac{1}{\sqrt{2}}\frac{4}{3}s^2\theta_W$, $g_V^{I=1} = \frac{1}{\sqrt{2}}(2 - 4s^2\theta_W)$, $g_V^{s} = -1 + \frac{4}{3}s^2\theta_W$. Consequently, this isospin decomposition relates weak proton form factors to the proton and neutron electromagnetic form factors,

$$\langle p|J^{\mu}_{NC,V}|p\rangle = (1 - 4\sin^2\theta_W)\langle p|J^{\mu}_{em}|p\rangle - \langle n|J^{\mu}_{em}|n\rangle. \tag{A3}$$

Above, we neglected strangeness contributions that are generally small.

A similar relation is valid for $I = \frac{1}{2}$ resonances, as well:

$$\langle X|J^{\mu}_{NC,V}|p\rangle = (1 - 4\sin^2\theta_W)\langle X|J^{\mu}_{em}|p\rangle - \langle X|J^{\mu}_{em}|n\rangle. \tag{A4}$$

Then, the contribution of a resonance R with isospin $1/2$ to the interference γZ cross section can be related to its contribution to the electromagnetic cross section by

$$\begin{aligned} \langle p|J^{\mu}_{em}|R\rangle\langle R|J^{\mu}_{NC,V}|p\rangle = (1 - 4s^2\theta_W)\left|\langle R|J^{\mu}_{em}|p\rangle\right|^2 \\ - \langle p|J^{\mu}_{em}|R\rangle\langle R|J^{\mu}_{em}|n\rangle. \end{aligned} \tag{A5}$$

To proceed, we use the definition of the transition helicity amplitudes,

$$\begin{aligned} A^{p(n)}_{R,1/2}(W^2, Q^2) &= \langle R, \Lambda_R = 1/2|J^{\mu}_{em}(\lambda_\gamma = 1) \\ &\quad \times |p(n), \Lambda_N = -1/2\rangle, \\ A^{p(n)}_{R,3/2}(W^2, Q^2) &= \langle R, \Lambda_R = 3/2|J^{\mu}_{em}(\lambda_\gamma = 1) \\ &\quad \times |p(n), \Lambda_N = 1/2\rangle, \\ S^{p(n)}_{R,1/2}(W^2, Q^2) &= \langle R, \Lambda_R = 1/2|J^{\mu}_{em}(\lambda_\gamma = 0) \\ &\quad \times |p(n), \Lambda_N = 1/2\rangle, \end{aligned} \tag{A6}$$

where we introduced photon helicity $\lambda_\gamma = 0, \pm 1$, nucleon helicity $\Lambda_N = \pm 1/2$, and the helicity of the resonance R that is related to the former two as $\Lambda_R = \Lambda_N + \lambda_\gamma$. Resonance contributions to the total cross sections $\sigma_{T,L}$ are related to the helicity amplitudes as

$$\begin{aligned} \sigma_T^{\gamma p(\gamma n),R} &= \frac{2M}{M_R\Gamma_R}\left\{\left|A^{p(n)}_{R,1/2}\right|^2 + \left|A^{p(n)}_{R,3/2}\right|^2\right\}, \\ \sigma_L^{\gamma p(\gamma n),R} &= \frac{4M}{M_R\Gamma_R}\frac{Q^2}{q_R^2}\left|S^{p(n)}_{R,1/2}\right|^2, \end{aligned} \tag{A7}$$

with M_R, Γ_R, and q_R the resonance mass, width and the three momentum of the virtual photon on the resonance position, respectively. In the above equation, the arguments W^2, Q^2 of the cross sections and helicity amplitudes were suppressed.

We combine the definition of Eq. (35) with Eqs. (A5), (A6), (A7) and finally obtain

$$\begin{aligned} \xi^R_{Z/\gamma}(Q^2) &= (1 - 4s^2\theta_W) - \frac{A^p_{R,\frac{1}{2}}A^{n*}_{R,\frac{1}{2}} + A^p_{R,\frac{3}{2}}A^{n*}_{R,\frac{3}{2}}}{\left|A^p_{R,\frac{1}{2}}\right|^2 + \left|A^p_{R,\frac{3}{2}}\right|^2}, \\ \zeta^R_{Z/\gamma}(Q^2) &= (1 - 4s^2\theta_W) - \frac{S^n_{R,\frac{1}{2}}}{S^p_{R,\frac{1}{2}}}. \end{aligned} \tag{A8}$$

For spin-$\frac{1}{2}$ resonances, only $A^{p,n}_{1/2}$ pieces contribute in the transverse ratios $\xi^R_{Z/\gamma}$. To a good approximation, the width and position of a resonance can be assumed to be the same for proton- and neutron-induced reactions. In this case, the W dependence cancels out in the ratio, and it is a function of Q^2 only.

We write in general

$$\begin{aligned} \xi^R_{Z/\gamma}(Q^2) &= (1 - 4s^2\theta_W) - y_R \times x_R(Q^2), \\ \zeta^R_{Z/\gamma}(Q^2) &= (1 - 4s^2\theta_W) - \tilde{y}_R \times \tilde{x}_R(Q^2), \end{aligned} \tag{A9}$$

with y_R ($\tilde{y}_R$) the values of the ratio of the neutron and proton transverse (longitudinal) helicity amplitudes in Eq. (A6) at $Q^2 = 0$ and x_R ($\tilde{x}_R$) the respective form factors. The form factors are normalized to unity at the real photon point.

For the resonances of isospin 3/2, the transition is purely isovector, and the ratio of the cross sections is given by $\frac{g_V^{I=1}}{q^{I=1}} = 2 - 4\sin^2\theta_W$ and is Q^2-independent. However, for the phenomenological analyses of the inclusive virtual photoabsorption data on the proton and neutron, Refs. [38,42] widely used in this work, this rule does not hold. For the $\Delta(1232)$ it holds to about 10%. For the $F_{37}(1950)$, the proton and neutron transition form factors show very different behavior (monopole for the proton vs dipole for the neutron). Furthermore, the unnaturally mild monopole form factor raises a question of whether this contribution should be considered as part of the background where monopole form factors arise naturally in the VDM picture. Correspondingly, rather than operate with a form factor $x_R(Q^2$ for the two isospin-3/2 resonances we assign an uncertainty to the ratios $y_R^{I=3/2} = -1$: 10% for the $\Delta(1232)$ and 100% for the $F_{37}(1950)$ and use $x_R(Q^2) = 1$ for both.

We next turn to the form factors $x_R(Q^2)$ of the isospin-1/2 resonances. To estimate these, one needs the Q^2 dependence of the transition helicity amplitudes for the excitation of these resonances. Unfortunately, the phenomenological fits

of Refs. [38,42] do not provide us with this information: They only give us $|A^{p(n)}_{R,1/2}|^2 + |A^{p(n)}_{R,3/2}|^2$ and $|S^{p(n)}_{R,1/2}|^2$. Instead, we need, for example, $A^{p}_{R,\frac{1}{2}} A^{n*}_{R,\frac{1}{2}} + A^{p}_{R,\frac{3}{2}} A^{n*}_{R,\frac{3}{2}}$. For spin-1/2 resonances, only $A_{1/2}$'s contribute. Then, one has for the second terms in Eq. (A8)

$$\frac{A^{p}_{R,\frac{1}{2}} A^{n*}_{R,\frac{1}{2}}}{\left|A^{p}_{R,\frac{1}{2}}\right|^2} = \pm\sqrt{\frac{\sigma_T^{\gamma n,R}}{\sigma_T^{\gamma p,R}}}\,,$$
$$\frac{S^{p}_{R,\frac{1}{2}} S^{n*}_{R,\frac{1}{2}}}{\left|S^{p}_{R,\frac{1}{2}}\right|^2} = \pm\sqrt{\frac{\sigma_L^{\gamma n,R}}{\sigma_L^{\gamma p,R}}}\,, \tag{A10}$$

and the only missing piece above is the relative sign of the proton and neutron helicity amplitudes. This sign is well defined and can be taken, for instance, from the PDG or from quark model [43]. For spin-3/2 resonances $D_{13}(1520)$ and $F_{15}(1680)$, the information provided by Refs. [38,42] is not sufficient to determine respective $x_R(Q^2)$. We can only approximately estimate those by noticing that for these resonances, the PDG suggests that the $p \to N^*$ transition is completely dominated by the $A_{3/2}$ helicity amplitude [40]. Then, we can adapt the same logic as for the spin-1/2 resonances, by substituting $A_{3/2}$'s in place of $A_{1/2}$'s in Eq. (A10).

However, this procedure cannot be considered reliable because such "extracted" form factors $x_R(Q^2)$ will contain a model dependence that is very hard to estimate. Instead, we use the following reasoning. We verified that with the approximations described above, the results of Refs. [38,42] lead to the form factors $x_R(Q^2)$ that differ from 1 by at most 10%–20% for values of $Q^2 \leqslant 0.6 - 0.8$ GeV^2 for all five isospin-1/2 resonances. At the same time, the PDG quotes the errors for the helicity amplitudes [40] for the excitation of those resonances that are conservative enough to accomodate this 10%–20% discrepancy. Indeed, the PDG values represent an average over world data and over various analyses; therefore, the errors that they quote contain not only the statistical and systematic error of each experiment, but also the systematic error owing to model dependence of those analyses. This means that at low values of Q^2, the error introduced if setting $x_R(Q^2) \approx x_R(0) = 1$ is reasonably small as compared to the error in the respective y_R. While at larger values of Q^2 this is not the case any longer, owing to resonance form factors the impact of these values of Q^2 on the dispersion correction $\Box_{\gamma Z}$ is small. From the discussion of the results, we see that

(i) the resonance contribution is dominated by the $\Delta(1232)$ for which the issue of the uncertainty in $x_R(Q^2)$ is controlled within 10%, as discussed earlier;
(ii) the overall uncertainty on the resonance contribution is dominated by that owing to the problem of the identification of the high-lying resonance in the analysis of Bosted and Christy with the $F_{37}(1950)$;
(iii) the total uncertainty in the dispersion correction $\Box_{\gamma Z}$ is dominated by the uncertainty owing to the background contribution. Then, even doubling the uncertainty in the contribution of the $S_{11}(1535)$ owing to $x_R(Q^2)$ will not significantly change our overall conclusions.

This allows us to set all $x_R(Q^2) = 1$ for all seven resonances considered here (including the isospin-3/2 resonances discussed earlier). The error introduced by this approximation is safely covered by using the conservative PDG errors for the resonance helicity amplitudes.

Finally, we discuss the ratios of the longitudinal cross sections $\zeta^R_{Z/\gamma}$. In Ref. [42], it was shown that the hypothesis that the ratio of the resonance contributions to longitudinal and the transverse cross sections for the proton and for the neutron target are equal is well supported by the experimental data. Although this conclusion is model-dependent, as well, the general impact of the longitudinal cross section on the $\Box_{\gamma Z}$ was found to be very small. This allows us to use the assumption of Ref. [42] here and set $\zeta^R_{Z/\gamma} = \xi^R_{Z/\gamma}$ for all seven resonances. As a result, we arrive at Eq. (37) with $\xi^R_{Z/\gamma} = 1 - 4\sin^2\theta_W - y_R$, where the values of y_R are listed in Table III.

[1] J. Erler and M. J. Ramsey-Musolf, Prog. Part. Nucl. Phys. **54**, 351 (2005).
[2] M. J. Ramsey-Musolf and S. Su, Phys. Rept. **456**, 1 (2008).
[3] M. J. Ramsey-Musolf, Phys. Rev. C **60**, 015501 (1999).
[4] R. D. Young, R. D. Carlini, A. W. Thomas, and J. Roche, Phys. Rev. Lett. **99**, 122003 (2007).
[5] J. Erler, A. Kurylov, and M. J. Ramsey-Musolf, Phys. Rev. D **68**, 016006 (2003).
[6] W. T. H. Van Oers (QWEAK Collaboration), Nucl. Phys. A **790**, 81 (2007).
[7] J. Erler and M. J. Ramsey-Musolf, Phys. Rev. D **72**, 073003 (2005).
[8] W. J. Marciano and A. Sirlin, Phys. Rev. D **27**, 552 (1983); **29**, 75 (1984); **31**, 213 (1985).
[9] C. E. Carlson and M. Vanderhaeghen, Ann. Rev. Nucl. Part. Sci. **57**, 171 (2007).
[10] M. J. Musolf and B. R. Holstein, Phys. Lett. B **242**, 461 (1990).
[11] M. Gorchtein and C. J. Horowitz, Phys. Rev. Lett. **102**, 091806 (2009).
[12] H. Q. Zhou, C. W. Kao, and S. N. Yang, Phys. Rev. Lett. **99**, 262001 (2007); **100**, 059903 (2008).
[13] K. Nagata, H. Q. Zhou, C. W. Kao, and S. N. Yang, Phys. Rev. C **79**, 062501 (2009).
[14] Y. C. Chen, C. W. Kao, and M. Vanderhaeghen, arXiv:0903.1098 [nucl-th].
[15] A. Sibirtsev, P. G. Blunden, W. Melnitchouk, and A. W. Thomas, Phys. Rev. D **82**, 013011 (2010).
[16] M. Gorchtein, C. J. Horowitz, and M. J. Ramsey-Musolf, AIP Conf. Proc. **1265**, 328 (2010).
[17] B. C. Rislow and C. E. Carlson, arXiv:1011.2397.
[18] M. K. Jones *et al.*, Phys. Rev. Lett. **84**, 1398 (2000); O. Gayou *et al.*, *ibid.* **88**, 092301 (2002); V. Punjabi *et al.*, Phys. Rev. C **71**, 055202 (2005); **71**, 069902 (2005); M. E. Christy *et al.*, *ibid.* **70**, 015206 (2004); I. A. Qattan *et al.*, Phys. Rev. Lett. **94**, 142301 (2005).

[19] M. J. Ramsey-Musolf, Phys. Rev. C **60**, 015501 (1999).
[20] J. A. Tjon, P. G. Blunden, and W. Melnitchouk, Phys. Rev. C **79**, 055201 (2009).
[21] J. J. Sakurai, Ann. Phys. **11**, 1 (1960); M. Gell-Mann and F. Zachariasen, Phys. Rev. **124**, 953 (1961); M. Gell-Mann, D. Sharp, and W. G. Wagner, Phys. Rev. Lett. **8**, 261 (1962); T. H. Bauer *et al.*, Rev. Mod. Phys. **50**, 261 (1978); **51**, 407(E) (1979).
[22] V. N. Gribov, Sov. Phys. JETP **29**, 483 (1969); **30**, 709 (1970); J. J. Sakurai and D. Schildknecht, Phys. Lett. B **40**, 121 (1972).
[23] E. D. Bloom *et al.*, SLAC-PUB-0653 (1969).
[24] T. A. Armstrong *et al.*, Phys. Rev. D **5**, 1640 (1972).
[25] D. O. Caldwell *et al.*, Phys. Rev. D **7**, 1362 (1973).
[26] D. O. Caldwell *et al.*, Phys. Rev. Lett. **40**, 1222 (1978).
[27] S. Chekanov *et al.* (ZEUS Collaboration), Nucl. Phys. B **627**, 3 (2002).
[28] G. M. Vereshkov, O. D. Lalakulich, Yu. F. Novoseltsev, and R. V. Novoseltseva, Phys. Atom. Nucl. **66**, 565 (2003).
[29] Y. Liang *et al.* (JLab Hall C E94-110 Collaboration), arXiv:nucl-ex/0410027.
[30] Preliminary results from JLab E00-002, C. Keppel and M. I. Niculescu, spokespersons, data available at [hallcweb.jlab.org/resdata].
[31] L. W. Whitlow *et al.*, Phys. Lett. B **282**, 475 (1992).
[32] Adams *et al.* (E665 Collaboration), Phys. Rev. D **54**, 3006 (1996).
[33] C. Adloff *et al.* (H1 Collaboration), Eur. Phys. J. C **21**, 33 (2001).
[34] J. Breitweg *et al.* (ZEUS Collaboration), Eur. Phys. J. C **7**, 609 (1999); B. Surrow, *ibid.* **2**, 1 (1999).
[35] N. Bianchi *et al.*, Phys. Rev. C **54**, 1688 (1996).
[36] C. Amsler *et al.*, Phys. Lett. B **667**, 1 (2008).
[37] G. Cvetic, D. Schildknecht, B. Surrow, and M. Tentyukov, Eur. Phys. J. C **20**, 77 (2001); G. Cvetic, D. Schildknecht, and A. Shoshi, *ibid.* **13**, 301 (2000);
[38] M. E. Christy and P. E. Bosted, Phys. Rev. C **81**, 055213 (2010).
[39] J. Alwall and G. Ingelman, Phys. Lett. B **596**, 77 (2004).
[40] K. Nakamura *et al.* (Particle Data Group), J. Phys. G **37**, 075021 (2010).
[41] For recent experimental results and references to earlier measurements, see, for example, D. Androic *et al.* (G0 Collaboration), Phys. Rev. Lett. **104**, 012001 (2010); A. Acha *et al.* (HAPPEX Collaboration), *ibid.* **98**, 032301 (2007); S. Baunack *et al.*, *ibid.* **102**, 151803 (2009).
[42] P. E. Bosted and M. E. Christy, Phys. Rev. C **77**, 065206 (2008).
[43] R. Koniuk and N. Isgur, Phys. Rev. D **21**, 1868 (1980).
[44] L. Stodolsky, Phys. Rev. Lett. **18**, 135 (1967).
[45] S. Chekanov *et al.*, (ZEUS Collaboration) Nucl. Phys. B **627**, 3 (2002).
[46] J. Breitweg *et al.* (ZEUS Collaboration), Phys. Lett. B **487**, 273 (2000).
[47] F. Maas (private communication).
[48] A. V. Afanasev and N. P. Merenkov, Phys. Lett. B **599**, 48 (2004); Phys. Rev. D **70**, 073002 (2004).
[49] M. Gorchtein, Phys. Lett. B **644**, 322 (2007).
[50] M. Gorchtein and C. J. Horowitz, Phys. Rev. C **77**, 044606 (2008).
[51] A. S. Aleksanian *et al.*, Sov. J. Nucl. Phys. **45**, 628 (1987).
[52] S. J. Pollock, E. N. Fortson, and L. Wilets, Phys. Rev. C **46**, 2587 (1992).